Science
AAAS

Supplementary Materials for

Inhibition of nonalcoholic fatty liver disease in mice by selective inhibition of mTORC1

Bridget S. Gosis *et al*.

Corresponding author: Zoltan Arany, zarany@pennmedicine.upenn.edur

Science **376**, eabf8271 (2022)
DOI: 10.1126/science.abf8271

The PDF file includes:

Materials and Methods
Figs. S1 to S12
Table S1
References

Other Supplementary Material for this manuscript includes the following:

MDAR Reproducibility Checklist

Materials and Methods

Animal Studies

All animal studies were approved by the University of Pennsylvania Institutional Animal Care and Use Committee. Mice were housed on a normal light-dark cycle (light on from 7 am to 7 pm) with constant access to normal chow (LabDiet, 5010) and water, except for special diets or periods of fasting where specified. Experiments were initiated on mice of 6-13 weeks (typically 7-8 weeks) of age, unless otherwise stated. All experiments were performed with littermate controls. All mouse procedures were approved by the University of Pennsylvania Animal Care and Use Committee. Most studies involved either homozygous *Flcn*$^{lox/lox}$ mice (*14*, *54*) or *Flcn*$^{lox/lox}$ mice also containing a loss-of-function whole-body *Tfe3* mutation (*14*, *45*). One breeding pair can yield 4 genotypes of mice: "control", liver *Flcn* KO ("LiFKO"), *Tfe3* whole-body knockout ("*Tfe3* KO"), and liver *Flcn* KO and *Tfe3* whole-body knockout together (double knockout, or "DKO"). To do this, we first cross *Flcn*$^{lox/lox}$; *Tfe3*$^{+/Y}$ males (*Tfe3* is X-linked, so these are wild-type for TFE3) with *Flcn*$^{lox/lox}$; *Tfe3*$^{+/-}$ females, to yield males that are *Flcn*$^{lox/lox}$ and either *Tfe3*$^{+/Y}$ (wild-type for *Tfe3*) or *Tfe3*$^{-/Y}$ (KO for *Tfe3*).

For most experiments (with the exception of the experiments described at the end of this section), these male mice were fed on normal chow (LabDiet, 5010) until adulthood then injected with ~1.5e11 genome copies/mouse of AAV8-TBG-GFP or AAV8-TBG-Cre (Penn Vector Core, AV-8-PV0146 and AV-8-PV1091) to yield control mice (*Flcn*$^{lox/lox}$, *Tfe3*$^{+/Y}$ with GFP), LiFKO mice (*Flcn*$^{lox/lox}$, *Tfe3*$^{+/Y}$ with Cre), Tfe3 KO mice (*Flcn*$^{lox/lox}$, *Tfe3*$^{-/Y}$ with GFP), and DKO mice (*Flcn*$^{lox/lox}$, *Tfe3*$^{-/Y}$ with Cre). Further experiments were subsequently begun about one week (occasionally 2-4 weeks) after virus injection and consisted of the following experimental paradigms (1) Mice were fed normal chow (LabDiet, 5010) and normal water, and euthanized either ad lib in the morning/afternoon (Fig. 1E, S7A, 3G, and normal chow ChIP-seq experiments) or after an overnight fast followed by 4 hours of normal chow refeeding (Fig. 1D, 1G, S1B). Livers were harvested for downstream analysis. Of note, the livers that were analyzed for DNL gene expression (Fig. S7A) were from mice that were injected with AAV at a range of 12 weeks to 6.5 months of age. (2) Mice were fed 7-9 days of FPC diet regimen, consisting of FPC diet chow (*30*) (Teklad, TD190142) as well as 42 g/L glucose (55%) and fructose (45%) in the drinking water, and euthanized after either an overnight fast followed by 4 hours of FPC diet regimen refeeding (diet: Teklad, TD190142) or ad lib at around 10 pm (Fig. 1H, 1I, 5A-C, S1C, S8B). Of note, FPC diet chow was always given with sugar water. (3) Mice were fed 16 weeks of normal chow or AMLN diet (*28*) (Research Diets, D09100301) and consequently underwent an oral GTT (see more details below). The mice were then fed 1-2.5 more weeks of normal chow and AMLN diet and euthanized after a 4-6 hour fast (Fig. 2A-E, 3A-C, 3E, 4A-B, S2B-F, S2H-J, S5A-B, S8A-B, S12A, S12C). (4) Mice were fed 16 weeks of normal chow/normal water or an FPC diet/sugar water regimen (diet: Teklad, TD160785, FPC diet as mentioned before but with vitamin-free casein) and euthanized after removing their food (but not their normal or sugar water) for ~4-6 hours (Fig. 2F-J, 3D, 4C-D, S4C-G, S8B, S12B, S12D). (5) Mice were fed 5-6 days of GAN diet (Research Diets, D09100310), then subjected to a GTT as described below (Fig. S5C). The same mice were fed an additional 4-5 days of GAN diet then underwent a CLAMS experiment (Fig. S3, S6C). The mice were

continued on diet then euthanized at ~8 weeks of feeding after a 5 hour fast (Fig. S2G). (6) Mice fed on normal chow underwent a CLAMS experiment, then fed on 10 days of FPC diet regimen and subjected to an additional CLAMS experiment (Fig. S3, S4A-B, S6C). After 2.5 weeks of FPC diet feeding, mice were fasted overnight and plasma was collected for beta-hydroxybutyrate analysis (Fig. S6A). (7) Mice were fed 7-11 days of AMLN diet, and consequently underwent the ^{13}C fructose gavage experiment, as described below (Fig. 4E). (8) Mice on normal chow underwent the ^{13}C fructose gavage experiment, as described below (Fig. S7B). (9) For the D_2O experiment, mice were fed 9 days of FPC diet regimen, then injected with D_2O and euthanized starting at midnight, in the fed state, as detailed below (Fig. 4F). Plasma was also collected for analysis of beta-hydroxybutyrate (Fig. S6A). (7) For the LXR agonist rescue experiment, mice were fed ~7.5-9.5 weeks of the FPC diet regimen (diet: Teklad, TD190142) with twice weekly vehicle or T0901317 injections and subsequently euthanized ad lib in the morning, all as described below (Fig. S8C-E). (9) For the NASH protection experiment, mice were fed 6 weeks of normal chow or CDAA-HF diet (*47*) (Research Diets, A06071302), and euthanized after a 4-6 hour fast (Fig. 6A-E, S11).

Other experiments deviated from the above injection scheme. For AAV-nSREBP-1c experiments, male mice fed on normal chow were given either 2.5e11 genome copies/mouse of AAV8-TBG-GFP (control mice given control virus, referred to as "control"), 2.5e11 genome copies/mouse of AAV8-TBG-Cre (LiFKO mice given control virus, referred to as "LiFKO"), 1.5e11 genome copies/mouse of AAV8-TBG-GFP + 1.0e11 genome copies/mouse of AAV8-ApoE/AAT-nSREBP-1c (control mice given nSREBP-1c virus, referred to as "control+1c"), or 1.5e11 genome copies/mouse of AAV8-TBG-Cre + 1.0e11 genome copies/mouse of AAV8-ApoE/AAT-nSREBP-1c (LiFKO mice given nSREBP-1c virus, referred to as "LiFKO+1c"). About a week after virus injection, mice were fed 9 days of FPC diet regimen (diet: Teklad, TD190142) then euthanized ad lib around 9-10 am (Fig. 5F-J and FPC diet ChIP-seq experiments). For the NASH reversal experiment, *Flcn*$^{lox/lox}$ male mice were fed 29 days of CDAA-HF diet, to induce NASH. Some were euthanized after a ~4-hour fast (non-injected). The rest were injected with either 1.5e11 GC/mouse of AAV8-TBG-GFP or -Cre, fed another 4 weeks of CDAA-HF diet, and subsequently euthanized after a ~4-hour fast (Fig. 6F-J, S11). For the control vs. *Raptor* KO subcellular fractionation experiment, mouse liver samples from the laboratory of Dr. Paul Titchenell were used. 6-10 week old *Raptor*$^{lox/lox}$ mice were fed normal chow and injected with 1.0e11 GC/mouse of either AAV8-TBG-GFP (control) or -Cre ("*Rap* KO" or "*Raptor* KO"), and euthanized 2 weeks later after an overnight fast followed by 4 hours of refeeding, as referenced in Quinn *et al.*, 2017 (Fig. 1F, S1A). For the control vs. *Tsc1* KO subcellular fractional experiment, mouse liver samples from the laboratory of Dr. Sudha Biddinger were used. 8-9 week old female *Tsc1*$^{lox/lox}$ (control) mice or Albumin-Cre *Tsc1*$^{lox/lox}$ mice (*Tsc1* KO) (*63*) were euthanized ad lib (Fig. 1J, S1D).

Protein isolation from whole tissues.

A small chunk of liver was combined with a steel bead and 1 mL of RIPA buffer (homemade or RPI R26200) containing cOmplete Mini, EDTA-free protease inhibitor (Roche, 11836170001) and PhosSTOP phosphatase inhibitor (Roche, 4906837001). The liver was then homogenized using the TissueLyser LT machine (Qiagen, 85600) at a

frequency of 50 Hz for 5 minutes followed by probe sonication, or using the Omni Bead Ruptor 12 (Omni, SKU 19-050A) at a setting of 3.25 speed for 20 seconds, repeated twice. The mixture was spun at 10 minutes at maximum speed (~14,000 rpm) at 4 ºC, to pellet debris. The supernatant was then collected into a fresh tube, taking care to avoid any top lipid layer. If the lipid layer was disturbed, then the tubes were re-spun, and lipid-free supernatant was collected again. Protein concentration was measured with BCA protein assay kit (Thermo Fisher, 23225) and protein concentrations were adjusted to the same concentration per sample.

Immunoblotting

The same amount of protein (5-16.66 µg) per sample was loaded to a 4-20% gradient Tris-polyacrylamide gel (Bio-Rad, 3450034) and electrophoresed at 100V for 1-1.5 hours. The gels were transferred to PVDF membranes (IPVH00010) at 500 mA for 60-80 minutes, which were then blocked in 5% non-fat dry milk in TBST for 30-60 minutes and incubated with primary antibody overnight at 4 ºC. The next day, membranes were washed in TBST, and then incubated for 30-60 minutes with rabbit (Cell Signaling Technology, 7074) or mouse (Cell Signaling Technology, 7076) horseradish peroxidase (HRP)-conjugated secondary antibody diluted at 1:10,000 in 5% non-fat dry milk in TBST. The membranes were washed again in TBST, incubated for ~30 seconds with enhanced chemiluminescent substrate for HRP (Thermo Fisher, 34094), and imaged using a digital imager (GE Healthcare Life Sciences, ImageQuant LAS 400; or Amersham Imager 600). The following primary antibodies were used: anti-FLCN (Abcam, ab124885), anti-HSP90 (Cell Signaling Technology, 4874), anti-TFE3 (Millipore Sigma, HPA023881), anti-14-3-3 (Cell Signaling Technology, 8312), anti-pS6 S240/4 (Cell Signaling Technology, 5364), anti-total S6 (Cell Signaling Technology, 2217), anti-pS6K Thr389 (Cell Signaling Technology, 9234), anti-total S6K (Cell Signaling Technology, 2708), anti-p4E-BP1 S65 (Cell Signaling Technology, 9451), anti-p4E-BP1 Thr37/46 (Cell Signaling Technology, 2855), anti-total 4E-BP1 (Cell Signaling Technology, 9644), anti-total Lipin1 and anti-pLipin1 S106 (*8*), anti-beta actin (Cell Signaling Technology, 4970), anti-HDAC2 (Abcam, ab32117), anti-pAMPK T172 (Cell Signaling Technology, 2535), anti-total AMPK (5831), anti-pACC S79 (Cell Signaling Technology, 11818), anti-total ACC (Cell Signaling Technology, 3676), anti-pULK1 S555 (Cell Signaling Technology, 5869), anti-total ULK1 (Cell Signaling Technology, 8054), anti-pAKT S473 (Cell Signaling Technology, 9271), anti-total AKT (Cell Signaling Technology, 4691), anti-OXPHOS cocktail (Abcam, ab110413), anti-LC3B (Abcam, ab192890), anti-FASN (Cell Signaling Technology, 3180), anti-ACSS2 (Cell Signaling Technology, 3658), anti-ACLY (Cell Signaling Technology, 13390), anti-SREBP1 (Millipore Sigma, MABS1987), anti-HA (Cell Signaling Technology, 3724), and anti-INSIG2 (*64*).

Quantification of immunoblots

Immunoblots were quantified using FIJI software. A rectangle of the same size was drawn around the band of interest in each lane, and another rectangle was drawn in an empty lane for a background measurement. Integrated density measurements were taken for each rectangle, and background integrated density was subtracted. For TFE3

immunoblot quantification, the rectangle included both the upper band, induced by LiFKO (at ~90 kDA), and the lower bands (at ~70 kDA).

Subcellular fractionation followed by protein isolation and immunoblotting: Control, LiFKO, and *Tfe3* KO livers

370-425.7 mg of liver was minced with scissors. 4 mL of hypotonic buffer (10 mM HEPES, 1.5 mM $MgCl_2$, 10 mM KCl, with 1 mM of DTT and protease/phosphatase inhibitors) was then added to the tissue, and dounced with 10 strokes of pestle A followed by 20 strokes of pestle B (dounce tissue grinder set, Millipore Sigma, D9063). The sample was then vortexed and incubated on ice for 15 minutes. 640 uL of 12.5% IGEPAL CA-630 was added to the tube and vortexed for 10 seconds. The liver homogenate was then filtered through a 100-micron filter, and 100 µL of lysate was taken for the whole cell lysate fraction. The rest of the mixture was centrifuged for 10 minutes at 4 ºC at 3000 pm. The supernatant was collected as the cytoplasmic fraction. The pellet (nuclear fraction) was resuspended in extraction buffer (20 mM HEPES, 1.5 mM MgCl2, 0.42 M NaCl, 0.2 mM EDTA, 25% glycerol, with 1 mM of DTT and protease/phosphatase inhibitors). The samples were incubated on ice for 30 minutes, vortexed at 10-minute intervals, and then spun at maximum speed for 30 minutes. The supernatant was collected as the nuclear fraction. The nuclear and whole cell lysate fractions were quickly sonicated, and subsequently all fractions were subjected to BCA protein assay for protein quantification. Whole cell lysate and cytoplasmic fractions were adjusted to 1 µg/µL, while the nuclear fraction as adjusted to 0.6 µg/µL with RIPA buffer. For immunoblotting, the same amount of protein was loaded for each sample in a fraction (8.33 µg for the whole cell and cytoplasmic fractions, 5 µg for the nuclear fraction); immunoblotting was then performed as described in the above section.

Subcellular fractionation followed by protein isolation and immunoblotting: Control, *Raptor* KO, and *Tsc1* KO livers

A chunk of liver was minced with scissors. The rest of the fractionation protocol was as described above except the volumes were halved for most samples. All fractions were subjected to BCA protein assay for protein quantification, and proteins were diluted with the appropriate buffer (hypotonic buffer for whole cell and cytoplasmic fractions; extraction buffer for nuclear fraction). For immunoblotting, the same amount of protein was loaded for each sample in a fraction (*Raptor* KO experiment: 8.33 µg for the whole cell and cytoplasmic fractions, 5 µg for the nuclear fraction; *Tsc1* KO experiment: 16.66 µg for all fractions); immunoblotting was then performed as described in the above section.

Total Lipin1 immunoprecipitation followed by immunoblotting. To conjugate antibodies, either (1) 3 µL of 0.247 mg/mL anti-total Lipin1 antibody (*8*) or (2) 0.247 µL of 3 mg/mL rabbig IgG isotype control (Thermo Scientific, 10500C) was mixed with 15 µL protein A agarose (Invitrogen, 15918014) and 1 mL of lysis buffer (25 mM Tris HCl, 1 mM EDTA, 1 mM EGTA, 0.1% Tween20, 1 mM DTT) containing 0.1% BSA, 1 cOmplete Mini, EDTA-free protease inhibitor (Roche, 11836170001), and 1 PhosSTOP phosphatase inhibitor (Roche, 4906837001). The mixture was rotated for 60 minutes at room temperature. During antibody conjugation, ~50 mg of liver was then homogenized

in 1 mL lysis buffer using the Omni Bead Ruptor 12 at a setting of 3.25 speed for 20 seconds, repeated twice. Liver lysates were then spun at 10 minutes at maximum speed (~14,000 rpm) at 4 ºC, to pellet debris. The supernatant was then collected into a fresh tube, taking care to avoid any top lipid layer. Protein concentration was measured with BCA protein assay kit (Thermo Fisher, 23225). After antibodies were conjugated to agarose beads, the beads were spun at 800g for 15 seconds, and supernatant was removed. 1 mL of lysis buffer was added to wash, and beads were then re-spun. 1.5 mg of liver lysate was added to the washed beads, and the mixture was rotated for 2 hours at 4 ºC, for immunoprecipitation. The beads were then washed again 3 times, and finally resuspended in 50 µL of lysis buffer containing 4x Laemmli protein sample buffer (Bio-Rad, 1610747) and 2-mercaptoethanol. To elute immunoprecipitated protein, the resuspended beads were heated to 70 ºC for 10 minutes, then supernatant was collected. 10 µL of protein was subsequently loaded onto a gel for immunoblot as described above.

Histology analysis

Liver tissues were fixed in 4% paraformaldehyde for at least 16 hours, then dehydrated into 100% ethanol. Tissues were subsequently embedded in paraffin by the CVI Histology Core and sectioned. H&E staining was performed with CAT Hematoxylin (Biocare Medical, CATHE-M) and Edgar Degas Eosin (Biocare Medical, THE-MM). Sirius Red staining was performed with 0.1% Direct Red (Millipore Sigma, 365548) and 0.1% Fast Green (Millipore Sigma, F72525) in a picric acid solution, followed by incubation in 0.5% acetic acid solution. Liver tissues were additionally placed in a plastic mold containing embedding media (optimal cutting temperature, OCT), and subsequently flash-frozen in a container of 2-methylbutane submerged in liquid nitrogen. Frozen blocks were sectioned with a cryostat and stained with Oil Red O (Abcam ab150678). For quantification of Sirius Red staining, 3-14 random areas of liver were imaged with the 20x objective (CDAA-HF prevention study) or the 10x objective (CDAA-HF reversal study). FIJI and ImageJ were used to quantify Sirius Red+ area. Images were split to RGB channels, and the green channel was thresholded with Yen automatic thresholding. %area was then quantified which corresponded to percent Sirius Red+ area.

Liver triglyceride quantification

A range of 12-110 mg of liver was combined with 10 µL/mg of 5% Igepal CA630 and a steel bead. The livers were then homogenized using the TissueLyser LT machine (Qiagen 85600) at a frequency of 50 Hz for 5 minutes or using the Omni Bead Ruptor 12 at a setting of 3.25 speed for 20 seconds, repeated twice. The samples were boiled for 10 minutes at 80 ºC, with intermittent vortexing, cooled to room temperature, and then re-boiled, for complete solubilization of triglycerides. Samples were spun at 10,000g for 10 minutes at 4 ºC, and supernatant (including lipid layer) was collected. The supernatants were re-spun to remove any remaining debris, and once again supernatants (including lipid layer) were collected. The samples were diluted 1:20 in water for triglyceride measurement. 5 µL of each triglyceride standard (serial 1:1 dilutions starting from 200 mg/dl, VWR, 10022-966) and sample was mixed with 200 µL of Infinity Triglyceride Reagent (Fisher Scientific, TR22421) in a clear 96 well plate, and then incubated for 15 minutes at room temperature in the dark. The plate was read at an absorbance of 540 nm, and a standard curve was calculated using linear regression. Sample readings were

interpolated onto the standard curve to determine triglyceride concentration of liver lysates (mg/dL). These values were divided by 10 to determine triglyceride amount per gram of liver homogenized (mg/g).

Blind scoring of mouse NAFLD/NASH pathology slides

A pathologist from the Penn Vet Comparative Pathology Core blindly scored paraffin-embedded liver H&E slides for NAFLD activity score (NAS), consisting of the sum of the scores for steatosis grade, lobular inflammation, and ballooning degeneration. Paraffin-embedded liver Sirius Red slides were used for scoring of fibrosis stage, as referenced. Scoring was done as referenced (*65*). Briefly, the following scoring criteria were used: Steatosis grade (<5% = score of 0; 5-33% = score of 1; >33%-66% = score of 2; >66% = score of 3); Lobular inflammation (no inflammatory foci = score of 0; <2 foci per 200x field = score of 1; 2-4 foci per 200x field = score of 2; >4 foci per 200x field = score of 3); Ballooning degeneration (none = score of 0; few/borderline = score of 1; many = score of 2); Fibrosis stage (none = score of 0; mild perisinusoidal fibrosis = score of 1A; moderate perisinusoidal fibrosis = score of 1B; portal/periportal fibrosis = score of 1C; perisinusoidal and portal/periportal fibrosis = score of 2; bridging fibrosis = score of 3; cirrhosis = score of 4). Of note, all livers studied either had fibrosis scores of 0 (no fibrosis) or 1A (mild perisinusoidal fibrosis). NAS scores of 2 or less do not meet criteria for NASH, whereas scores of 5 or greater indicate presence of NASH. NAS scores of 3-4 are in between cases: there was interobserver disagreement on whether the livers should be diagnosed as having no NASH, borderline steatohepatitis, or definitive NASH.

Quantification of plasma triglycerides, non-esterified fatty acids, and cholesterol species

For the normal chow vs. AMLN diet experiments, mice were fasted for 4 hours, and blood samples were collected by heparinized capillary tubes and centrifuged at 5000g at 4 ºC for 20 minutes. The plasma layer was collected and stored at -80 ºC until analysis. Plasma samples were analyzed by Axcel autoanalyzer (Alfa Wassermann Diagnostic Technologies). For the FPC diet experiments, retro-orbital blood was collected by heparinized capillary tubes from mice who had their food removed (but not their normal or sugar water) for 4-6 hours. Blood was centrifuged at 10,000g at 4 ºC for 10 minutes. The plasma layer was collected and stored at -80 ºC until analysis. For triglyceride measurements for these FPC diet samples, plasma was diluted 1:2, and standards were made using serial dilutions of a glycerol standard solution (Millipore Sigma, G7793). 5 µL of plasma sample or standard was then mixed with either 200 µL of Infinity Triglyceride Reagent (Fisher Scientific, TR22421) or Free Glycerol Reagent (Millipore Sigma F6428) on a clear 96 well plate. The plate was incubated at room temperature for 15 minutes and absorbance was read at 540 nm. Glycerol and triglyceride standard curves were then calculated using linear regression, and sample readings were interpolated onto the standard curve to determine glycerol or triglyceride concentrations. To account for potential background glycerol affecting triglyceride measurements, the measured glycerol concentration of each sample was subtracted from the measured triglyceride concentration, for a final plasma triglyceride concentration. For measurement of non-esterified fatty acids for these FPC diet samples, a colorimetric assay (BioVision, K612) was used on 3 microliters of plasma.

Insulin measurements

For the 16 week normal chow vs. AMLN diet experiment, mice were fasted overnight, and tail blood was collected by heparinized capillary tubes and centrifuged at 5000g at 4 ºC for 20 minutes. For the 16 week FPC diet experiment, retro-orbital blood was collected by heparinized capillary tubes from mice who had their food removed (but not their normal or sugar water) for 4-6 hours. Blood was centrifuged at 10,000g at 4 ºC for 10 minutes. The plasma layer was collected and stored at -80 ºC until analysis. Insulin levels were then measured by ELISA (Crystal Chem, 90080).

Quantification of blood/plasma glucose

For the 16 week normal chow vs. AMLN diet experiment, mice were fasted overnight then blood glucose was measured from tail blood via a glucometer. For the 16 week FPC diet experiment, retro-orbital blood was collected by heparinized capillary tubes from mice who had their food removed (but not their normal or sugar water) for 4-6 hours. Blood was centrifuged at 10,000g at 4 ºC for 10 minutes. The plasma layer was collected and stored at -80 ºC until analysis. Plasma glucose was analyzed using a colorimetric assay (Crystal Chem, 81692). For glucose tolerance tests, blood glucose was also measured from tail blood via glucometer.

Quantification of plasma beta-hydroxybutyrate

Blood was collected by heparinized capillary tubes from mice either fasted overnight (tail blood) or ad lib fed around midnight (retro-orbital blood). Blood was centrifuged at 10,000g at 4 ºC for 10 minutes. The plasma layer was collected and stored at -80 ºC until analysis. Plasma was diluted 1:10 for ad lib fed samples and 1:30 for overnight fasted samples, and then beta hydroxybutyrate was measured using a colorimetric assay kit (Cayman Chemical Company, 700190).

Radioactive palmitate tracing in isolated hepatocytes

Primary hepatocytes were isolated, cultured overnight, and subjected to radioactive palmitate tracing for fatty acid oxidation measurements as referenced (*42*). The cells were incubated with 125 μM ^{3}H-palmitate conjugated on BSA and 1 mM carnitine for an additional 2 hours with or without 100 μM etomoxir. The media was delipidated and $^{3}H_2O$ was measured by scintillation counting.

Oral glucose tolerance test

Mice were fasted overnight (Fig. S5B) or for 5 hours (Fig. S5C). The mice were then weighed and tail blood was collected to measure fasting glucose via a glucometer. Each mouse was gavaged with 20% D-Glucose (10 μL per gram of body weight; final dose: 2 g/kg). Blood glucose was then measured at serial time points as indicated.

Whole body metabolism measurements

Body composition (fat, lean, total mass) was measured via EchoMRI. The mice were then placed in metabolic cages via the Comprehensive Lab Animal Monitoring System (CLAMS) and monitored for 5 days. Energy expenditure, food consumption, water consumption, ambulatory activity levels, and locomotor activity levels were measured at around 40-minute intervals. Data for each mouse were collated into one

single file using CalR (*66*). The rest of the data processing was done using Python3. We excluded mice with several (5 or more) values less than -5 kilocalories of food intake from food or food-related calculations, as this indicated major food sensor issues. This ended up being 1 control and 1 LiFKO mice for normal chow; 2 LiFKO mice for FPC diet; and 2 LiFKO mice for GAN diet. We additionally excluded 1 value of -12 kilocalories of food consumption from 1 of the LiFKO mice in the GAN diet study, as this indicated a food sensor issue at this time point (all other values were included). 1 of the LiFKO mice in the normal chow cohort did not have a connected activity line for the first 27 hours of the study, so we did not include these measurements in activity calculations. Energy expenditure (kilocalories/hour) and respiratory exchange ratio (RER) values, recorded by 40-minute intervals, were then averaged over all of the light cycles of the study, all of the dark cycles, or the entire study overall (full day). For energy expenditure, ANCOVA was performed on these "per cycle" average values, using lean mass as a covariate. Student's t-test was used to analyze RER values, as these have been reported not to vary by weight (*66*). Caloric food intake (kcal) was calculated by taking the measured food intake from the calorimeter (in grams) and multiplying by the physiological caloric content of the diet (3.42 kcal/gram for normal chow, 4.49 kcal/gram for GAN diet, and 5 kcal/gram for FPC diet). Energy balance was calculated for every time interval by subtracting energy expenditure (kcal) from kilocalories consumed, which was defined as caloric food intake plus any kilocalories consumed from water (only relevant for the FPC diet regimen which included sugar water; 0.1638 kcal/milliliter of water consumed). For water consumption, food consumption, energy balance, and activity measurements, values were summed either for all of the light cycles, all of the dark cycles, or the entire study overall (full day). The values were then divided by the number of light cycles, dark cycles, or full days of the study. For water consumption, food consumption, and energy balance, ANCOVA was performed on these "per cycle" average values, using lean mass as a covariate. Student's t-test was used to analyze activity measurements, as these have been reported not to vary by weight (*66*). Values for each parameter were also plotted by each 40-minute interval in the study.

RNA isolation

A small chunk of liver (~50 mg) was combined with a steel bead and 1 mL of TRIzol (Thermo Fisher, 15596026) and homogenized using the TissueLyser LT machine at a frequency of 50 Hz for 5 minutes. The mixture was spun at 5 minutes at maximum speed (~14,000 rpm) at 4 ºC, to pellet debris. 800 µL of supernatant was then collected into a fresh tube and combined with 200 µL of extra TRIzol and 200 µL of chloroform. The tube was vortexed for 5 seconds and spun for 15 minutes at maximum speed at 4 ºC. 400 µL of the subsequent aqueous layer was collected in a fresh tube and combined with 400 µL of isopropanol and vortexed. The mixture was incubated for 10 minutes at room temperature, and then spun for 10 minutes at maximum speed at 4 ºC to pellet RNA. The RNA pellet was washed once with 70-80% ethanol, then resuspended in 100 µL of water and incubated for 15 minutes at 37 ºC. The RNA was consequently cleaned up with the RNeasy Mini kit (Qiagen, 74104): 350 µL of RLT and 250 µL 100% ethanol was added to the RNA, which was then loaded to a spin column and washed twice with either RPE or 80% ethanol. The RNA was finally eluted in 50-100 µL RNAse-free water and adjusted to 0.15-0.5 µg/µL concentration.

cDNA production and qRT-PCR

Around 0.9-2 ng of RNA was then used for cDNA production using the High-Capacity cDNA Reverse Transcription Kit (Fisher Scientific, 4368814) with RNAse inhibitor (Thermo Fisher, N8080119). cDNA was diluted 1:10, 1:25, or 1:50. For qRT-PCR, 2 µL of diluted cDNA was then combined with 2.5 µL dsDNA binding dye (SYBR green, etc.) and 0.5 µL of forward and reverse primer (3 µM each). The BioRad CX384 C1000 Thermal Cycler was used to run the qPCR reaction, which involved heating to 95 ºC for 3 minutes, followed by 40 cycles at 95 ºC for 15 seconds then 60 ºC for 30 seconds, and culminating with a melt curve reaction. For each sample, each CT value was normalized to the average CT amongst housekeeping genes (*36b4*, *Tbp*, and/or *Hprt*). For each gene, the resultant values were then normalized to the average CT amongst the biological replicates of control mice. These values (*x*) were then plugged into the formula 2^-*x* to calculate relative expression. qRT-PCR primers are listed in Table S1.

RNA-sequencing

RNA isolation was performed as above with the following differences: (1) liver homogenates were incubated at room temperature for 15 minutes in TRIzol before centrifugation, (2) samples were incubated with chloroform for 5 minutes at room temperature before centrifugation, (3) chloroform extraction was performed twice, and (4) the initial ethanol wash step was performed twice. Library preparation and sequencing was then conducted at GENEWIZ LLC. 15 µL of RNA at a concentration of 392.17 ng/µL to 625.78 ng/µL was submitted to GENEWIZ, and then subjected to RNA quantification using Qubit 2.0 Fluorometer (Life Technologies), followed by examination of RNA integrity with Agilent TapeStation 4200 (Agilent Technologies). Library preparation was conducted using the NEBNext Ultra RNA Library Prep Kit for Illumina (New England Biolabs, E7530), followed by quantification and examination of RNA integrity as above as well as quantitative PCR. The libraries were then pooled, clustered on 1 lane of a flowcell, and sequenced on the Illumina HiSeq instrument (4000 or equivalent). The samples were sequenced using a 2x150 base pair paired end method. The HiSeq Control Software was used for image analysis and base calling, and Illumina's bcl2fastq 2.17 software was used to make FASTQ files. For index sequence identification, up to one mismatch was allowed.

RNA-seq analysis

Trimmomatic v0.32 (*67*) was used to trim the adaptors and remove low-quality sequencing reads. STAR v2.6.0c (*68*) was used to align reads to the mm9 mouse genome assembly. Samtools v1.7 (*69*) view was used to filter aligned reads without a mapped mate and alignments with mapq score below 10(-F 4 -q 10). Counts per gene were quantified using Rsubread v1.6.1 (*70*) package's featureCounts function with Ensembl v.67 mm9 gene annotation file. Genes with <1 count per million (CPM) in less than a quarter of samples were removed. Limma v3.40.6 (*71*) voom function was used to $\log_2$ transform and normalize the count matrix. Limma was used to fit a linear model and perform differential gene expression analysis, creating $\log_2$(fold change) values between different genotypes. P-values were adjusted for multiple comparisons with the Benjamini–Hochberg procedure. Gene set enrichment analysis (GSEA) was then

performed using the CAMERA function (*72*) in the limma package with an inter-gene correlation value of 0.01, and using the C2 curated gene sets in the GSEA Molecular Signatures Database (MSigDB). To generate a volcano plot for differentially expressed genes between LiFKO and control livers in both normal chow and AMLN diet conditions, $\log_2$(fold change) was plotted against -$\log_{10}$(adjusted p value) using the EnhancedVolcano package (*73*) in R studio. Lysosomal (*74*) and mitochondrial (Broad, Reactome gene set TCA cycle and respiratory electron transport) (*75*) genes were signified in respective colors on the volcano plot. Heatmaps were generated with Morpheus software, visualizing normalized expression values.

Measurement of de novo lipogenesis by ^{13}C fructose gavage

Mice were fasted from 9-10 am to 7 pm, then refed for 2 hours and subsequently gavaged with a mixture of 1:1 ^{12}C D-glucose:^{13}C fructose (D-[UL-$^{13}C_6$] fructose; Omicron FRU-011; 2g/kg each). Mice were euthanized the next morning around 9-10 am and livers were flash frozen. ~20 mg of liver tissue was then saponified to extract lipids, which was then subjected to LC-MS as described (*76*). LC-MS yielded ion counts for isotopomers (*M*+*i*) of each fatty acid measured, with *M* being the parent ion mass and *i* having a range of 0 (no carbons labeled) to *n* (all carbons in that fatty acid labeled). For each isotopomer, ion counts were multiplied by *i*. These values were then added together for each fatty acid, divided by *n* and the total ion count, and then multiplied by 100 to yield %enrichment.

Measurement of de novo lipogenesis by D_2O injection

Mice were injected intraperitoneally with 30 microliters per gram of body weight of 99.9% D_2O (Sigma-Aldrich, 151882) with 0.9% NaCl. Injections began at 7 pm and lasted until 8:30 pm. 5 hours after each injection (from 12 am to 1:30 am), the mice were euthanized and livers were flash frozen. ~20 mg of liver tissue was then saponified to extract lipids, which was then subjected to LC-MS as described (*76*). LC-MS yielded ion counts for isotopomers (*M*+*i*) of each fatty acid measured, with *M* being the parent ion mass and *i* having a range of 0 (no hydrogens labeled) to *n* (all hydrogens in that fatty acid labeled). For each isotopomer, ion counts were multiplied by *i*. These values were then added together for each fatty acid, divided by *n* and the total ion count, and then multiplied by 100 to yield %enrichment.

Injections of LXR agonist or vehicle control

100 mg/mL T0901317 (Cayman Chemical, 71810; reconstituted in DMSO) was combined 1:1 with Cremophor (Millipore Sigma, 238470), and then combined 1:9 with 5% mannitol solution. A vehicle mixture constituted of 1:1 DMSO:Cremophor, then combined 1:9 with 5% mannitol solution, as described (*77*). The mice were then injected intraperitoneally with T0901317 or vehicle at a volume of 10 µL per gram of body weight (50 mg/kg of T0901317) and started on FPC diet regimen (diet: Teklad, TD190142). Mice were injected twice weekly (Monday/Tuesday or Friday), as described (*36*). The last injection was given at ~9.5 weeks of FPC diet feeding around 4-6 pm, and mice were then euthanized 14 hours 10 minutes later, and livers were flash frozen. A small number of mice were euthanized at 7.5 or 8.5 weeks given the COVID-19 pandemic.

Construction of AAV8-ApoE/AAT-HA-nSREBP-1c

A constitutively nuclear SREBP-1c, based on the sequence used in Papazyan *et al.*, 2016 (a gift from Dr. Mitch Lazar's lab), was tagged N-terminally with a 3xHA tag from the pLJC5-Tmem192-3xHA vector (Addgene 102930) (*78*) and was cloned into the pGG2 vector (a gift from Dr. Mauro Giacca) (*79*) downstream of a liver-specific promoter, consisting of the ApoE enhancer upstream of the human alpha 1-antitrypsin promoter). Cloning was done using the In-Fusion cloning system (Takara, 638909), and DNA was amplified using TOP10 electrocompetent cells (Thermo Fisher, C404010) and NucleoBond Xtra Maxi Plus EF kit (Takara, 740426.10). AAV8 was then produced using Penn Vector Core.

Normal chow TFE3 ChIP-seq

116-335 mg of liver was minced with scissors, dounced with 10 strokes of pestle A (Millipore Sigma, D9063) in 15 mL of swelling buffer (10 mM HEPES, 2 mM $MgCl_2$, 3 mM $CaCl_2$), and incubated on ice for 20 minutes. The livers were then dounced with 20 strokes of pestle B (Millipore Sigma, D9063) and 15 mL more of swelling buffer was added. The liver mixture was passed through a 100 micron filter and then spun down at 400g for 10 minutes at 4 ºC. The resulting pellet was resuspended in 5 mL of swelling buffer and 10% glycerol. The mixture was vortexed while 5 mL of lysis buffer (10% glycerol, 1% Igepal CA630, in swelling buffer) was added slowly. The samples were incubated on ice for 5 minutes, and then another 15 mL lysis buffer was added. Nuclei were then pelleted at 600g for 5 minutes at 4 ºC, washed once with 10 mL of lysis buffer, and the final nuclei pellet was resuspended in 1 mL of PBS. For fixation, 9 mL of PBS containing 0.28 mL 37% formaldehyde was then added and the samples were incubated at room temperature for 20 minutes with rotation. The fixation was quenched with 0.87 mL of 2.5 M glycine and then incubated at room temperature for 5 minutes. Nuclei were then spun down, washed once with 10 mL HiC lysis buffer (10 mM Tris HCl, 10 mM NaCl, and 0.2% Igepal CA639), and resuspended in 100 µL ChIP dilution buffer (50 mM HEPES, 155 mM NaCl, 1.1% Triton X-100, 0.11% NaDeoxycholate, 1 mM EDTA) with 0.1% SDS and protease inhibitor. The nuclei were then sonicated with the Diagenode Bioruptor for 30 minutes on the high setting with 30 seconds on and off. Samples were then spun at maximum speed for 15 minutes at 4 ºC, and the supernatant was transferred into a fresh tube. A BCA was performed and samples were then normalized to the lowest concentration sample. 100 µg of sonicated chromatin was diluted into 210 µL of ChIP dilution buffer with 0.1% SDS and protease inhibitor. 10 µL of that was then taken as the input after being added to 40 µL ChIP dilution buffer with 0.1% SDS and protease inhibitor as well as 200 µL SDS lysis buffer (50 mM Tris-HCl, 10 mM EDTA, 1% SDS), and this input mixture was stored at -20 ºC. The remaining 200 µL of sonicated chromatin was used for immunoprecipitation (IP): 8 µL of TFE3 antibody (Millipore Sigma, HPA023881 lot K115357) was added and the mixture was rotated at 4 ºC for 24 hours. Protein G sepharose beads (Abcam, ab193259) were then washed twice with PBS and resuspended in 2 volumes of blocking solution (0.5% BSA in PBS). 75 µL of beads were then added to each IP sample, which were then rotated for 2 hours at 4 ºC. Beads were pelleted at 500g for 30 seconds at 4 ºC and supernatant was discarded. Beads were then washed in different 1 mL amounts of buffer as follows: ChIP dilution buffer

followed by a 30 second spin at 500g, ChIP dilution buffer followed by a 5 minute spin, ChIP dilution buffer plus an additional 500 mM NaCl followed by a 5 minute spin, ChIP wash buffer (10 mM Tris, 250 mM LiCl, 0.5% Igepal CA630, 0.5% NaDeoxycholate, 1 mM EDTA) followed by a 5 minute spin, and finally TE followed by a 5 minute spin. After this final spin, the beads were resuspended in 250 µL SDS lysis buffer, and chromatin was eluted after a 15 minute incubation at 65 ºC followed by a 1 minute spin. Input and IP samples were then heated at 65 ºC overnight to reverse crosslinks. Samples were then spun at maximum speed for 2 minutes, and supernatant transferred to a fresh tube. 250 µL TE, 4 µL proteinase K (20 µg/µL) and 4 µL glycogen (20 µg/µL) were then added and samples were incubated at 37 ºC for 2 hours. 20 µL 5M NaCl was added to each sample and then transferred to a phase lock tube (VWR, 10847-800) with 500 µL phenol chloroform. Samples were shaken and spun at maximum speed for 5 minutes. The supernatant was transferred to a new phase lock tube and 500 µL chloroform was added. Samples were spun again at maximum speed for 5 minutes and supernatant was transferred to a new tube with 1 mL 100% ethanol and stored at -20 ºC for a few days. Samples were then spun at maximum speed for 30 minutes to pellet DNA, which was then washed with 750 µL 70% ethanol. Pellet was then resuspended in 50 µL TE and incubated at 37 ºC for 15-30 minutes.

FPC diet TFE3 and HA-nSREBP-1c ChIP-seq

Around 200 mg of liver was minced with scissors, dounced with 10 strokes of pestle A in 15 mL of swelling buffer (10 mM HEPES, 2 mM $MgCl_2$, 3 mM $CaCl_2$ with protease inhibitor), and incubated on ice for 20 minutes. The livers were then dounced with 20 strokes of pestle B and 15 mL more of swelling buffer was added. The liver mixture was passed through a 100 micron filter and then spun down at 400g for 10 minutes at 4 ºC. The resulting pellet was resuspended in 5 mL of swelling buffer and 10% glycerol with protease inhibitor. The mixture was vortexed while 5 mL of lysis buffer (10% glycerol, 1% Igepal CA630, in swelling buffer with protease inhibitor) was added slowly. The samples were incubated on ice for 5 minutes, and then another 15 mL lysis buffer was added. Nuclei were then pelleted at 600g for 5 minutes at 4 ºC, washed once with 10 mL of lysis buffer, and the final nuclei pellet was resuspended in 1 mL of PBS. For fixation, 9 mL of PBS containing 0.28 mL 37% formaldehyde was then added and the samples were incubated at room temperature for 20 minutes with rotation. The fixation was quenched with 0.87 mL of 2.5 M glycine and then incubated at room temperature for 5 minutes. Nuclei were then spun down, washed once with 10 mL HiC lysis buffer (10 mM Tris HCl, 10 mM NaCl, and 0.2% Igepal CA639 and protease inhibitor), and resuspended in 100 µL ChIP dilution buffer (50 mM HEPES, 155 mM NaCl, 1.1% Triton X-100, 0.11% NaDeoxycholate, 1 mM EDTA) with 0.1% SDS and protease inhibitor. The nuclei were then sonicated with the Diagenode Bioruptor for 30 minutes on the high setting with 30 seconds on and off. Samples were then spun at maximum speed for 15 minutes at 4 ºC, and the supernatant was transferred into a fresh tube. A BCA was performed and samples were then normalized to the lowest concentration sample. For input control, 10.476 µg of sonicated chromatin was diluted into a final volume of 50 µL of ChIP dilution buffer with 0.1% SDS and protease inhibitor, and added to 200 µL of SDS lysis buffer (50 mM Tris-HCl, 10 mM EDTA, 1% SDS), and this input mixture was stored at -20 ºC. 209.524 µg of sonicated chromatin

was used for each IP: the sample received either 8 µL of TFE3 antibody (Millipore Sigma, HPA023881 lot O118166) or 60 µL HA-agarose beads (Millipore Sigma, A2095). The IP's were rotated at 4 ºC overnight. For the TFE3 ChIP, protein G sepharose beads (Abcam, ab193259) were washed twice with PBS and resuspended in 2 volumes of blocking solution (0.5% BSA in PBS). 75 µL of beads were then added to each IP sample, which were then rotated for 2 hours at 4 ºC. Both sets of IP samples were then spun at 500g for 30 seconds at 4 ºC to pellet sepharose/agarose beads, and supernatant was then discarded. Beads were then washed in different 1 mL amounts of buffer with rotation at 4 ºC for different amounts of time as follows, all followed by a 30 second spin at 500g at 4 ºC: ChIP dilution buffer briefly, ChIP dilution for 5 minutes, ChIP dilution buffer containing 500 mM NaCl (instead of the usual 155 mM NaCl) for 5 minutes, ChIP wash buffer (10 mM Tris, 250 mM LiCl, 0.5% Igepal CA630, 0.5% NaDeoxycholate, 1 mM EDTA) for 5 minutes, and finally TE for 5 minutes. After this final spin, the beads were resuspended in 250 µL SDS lysis buffer, and chromatin was eluted after a 15 minute incubation at 65 ºC followed by a 1 minute spin. Input and IP samples were then heated at 65 ºC overnight to reverse crosslinks. Samples were then spun at maximum speed for 2 minutes, and supernatant transferred to a fresh tube. 250 µL TE, 4 µL proteinase K (20 µg/µL) and 4 µL glycogen (20 µg/µL) were then added and samples were incubated at 37 ºC for 2 hours. 20 µL 5M NaCl was added to each sample and then transferred to a phase lock tube (VWR, 10847-800) with 500 µL phenol chloroform. Samples were shaken and spun at maximum speed for 5 minutes. The supernatant was transferred to a new phase lock tube and 500 µL chloroform was added. Samples were spun again at maximum speed for 5 minutes and supernatant was transferred to a new tube with 1 mL 100% ethanol and stored at -20 ºC for 1 hour. Samples were then spun at maximum speed for 30 minutes to pellet DNA, which was then washed with 750 µL 70% ethanol. Pellet was then resuspended in 50 µL TE and incubated at 37 ºC for 15-30 minutes.

ChIP-seq library preparation and sequencing

ChIP input and IP DNA was measured with the Qubit dsDNA high sensitivity kit (Thermo Fisher, Q32854), and then subjected to library prep based on that concentration using the NEBNext Ultra II DNA Library Prep Kit for Illumina (E7645S). NEBNext set 1 and 2 indexes (E7335S and E7500S) were used. Library fragment sizes were assessed with high sensitivity Bioanalyzer assay (Agilent, 5067-4626). To remove any remaining high molecular weight peaks, libraries were size selected an additional time: 37.5 µL (0.75x volume) of Ampure XP beads (Beckman Coulter, A63880) or RNAClean XP (Beckman Coulter, A63987) beads were added to 50 µL of library. Samples were incubated for 5 minutes at room temperature, placed on a magnetic rack, and the beads were discarded. To the remaining supernatant, 7.5 µL of more beads were added (0.15x volume). After another incubation, the supernatant was discarded. The beads were washed and ultimately resuspended in 30 µL of 0.1x TE buffer. The subsequent libraries were analyzed for fragment size with Bioanalyzer using the Agilent High Sensitivity DNA kit, and DNA concentration was measured using Qubit dsDNA HS assay. The libraries were subsequently pooled, using the same DNA amount per library, determined by the library with the lowest concentration. Pooled libraries were subsequently quantified using NEBNext Library Quant Kit for Illumina (New England Biolabs,

E7630S). 20 picomoles of pooled library DNA was subsequently denatured in a 1:1 ratio of 0.2N NaOH and incubated for 5 minutes at room temperature. 200 mM Tris was then added to the mixture (1:1 ratio of Tris to starting library volume). The denatured libraries were then diluted to 20 pM with HT1 Hybridization Buffer (Illumina, 20024906), and subsequently diluted to 1.8 pM in HT1. The final libraries were then sequenced using the NextSeq 500/550 High output Kit v2.5 (75 cycles) (Illumina, 20024906) using single-read sequencing on a NextSeq 550.

Normal chow TFE3 ChIP-seq analysis

Trimmomatic (v0.32) was used to trim the adaptors and remove low-quality sequencing reads in FASTQ files. Reads were aligned to the mm9 reference genome using Bowtie2 v2.2.8 (*80*) to generate bam files. The bam files were sorted and duplicates were consequently removed via Samtools (v1.7). Bam files were then converted to bed files by bedtools v2.27.0 and v2.27.1 (*81*); reads aligning to blacklist regions (*82*) and to chrM were also removed. Tag directories were then generated for each sample using HOMER v4.11 (*83*). The HOMER program getDifferentialPeaksReplicates.pl (v4.11) was used twice for each genotype group (control and LiFKO) to call peaks (using default settings: at least a fold-change of 4 and FDR of 0.001) over either (1) each genotype's respective input sample or (2) the 2 TFE3 ChIP samples done in the *Tfe3* KO genotype. The option -all was used on this program to output all peaks called. The 2 peaksets were then merged using mergePeaks (HOMER, v4.11), and overlapping peaks were designated as the final peakset for each genotype. Enriched motifs were found in the above peaksets via findMotifsGenome.pl (HOMER, v4.11). Motif HTML files were cleaned up using the Beautiful Soup python library, then a screenshot was taken for visualization. Enriched pathways were found in the peaksets via findGO.pl (HOMER, v4.11); specifically the most enriched Reactome pathways were depicted in this paper. bedGraph files were generated using HOMER, normalized to 1e7 reads per sample and input control, and the bedGraphtoBigWig v4 (*84*) program was used to create a bigWig file. WashU Epigenome Browser (*85*) was used for visualization of these bigWig files. To determine TFE3 enrichment at normal chow nSREBP-1c peaks, publicly available nSREBP-1c peaks (GSM2287950) were annotated using HOMER annotatepeaks.pl. Then, using the -hist option on annotatePeaks.pl, TFE3 enrichment (in 10 bp bins) was determined surrounding (1) all nSREBP-1c peaks, (2) just peaks within 5kb of a TSS, and (3) peaks within 5kb of TSS's of de novo lipogenesis genes (specifically, *Fasn*, *Mlxipl*, *Srebf1*, *Scd1*, *Acaca*, *Acacb, Acly*, *Acss2*); enrichment was calculated within 1000 bp from peak center, using TFE3 bedGraph files. TFE3 enrichment (within 1000 bp from peak center) on all GSM2287950 nSREBP-1c peaks was also determined with deepTools v3.3.0 (*86*) using the computeMatrix (reference-point mode) and plotHeatmap commands on TFE3 bigWig files.. Other publicly available liver ENCODE ChIP-seq bigwig files were also visualized on the WashU Epigenome Browser, namely PolII (GSM918738; GSE49847), H3K27ac (GSM1000140; GSE31039), H3K4me1 (GSM769015; GSE31039), H3K4me3 (GSM769014; GSE31039), and H3K9ac (GSM1000153; GSE31039).

FPC diet TFE3 and HA-nSREBP-1c ChIP-seq analysis

Trimmomatic (v0.36) was used to trim the adaptors and remove low-quality sequencing reads in FASTQ files. The quality of trimmed reads was checked using

FASTQC (v0.11.7). Reads were aligned to the mm9 reference genome using Bowtie2 v2.2.6 to generate bam files. The bam files were sorted and duplicates were consequently removed via Samtools (v0.1.19). Bam files were then converted to bed files via bedtools2 v2.25.0; reads aligning to blacklist regions and to chrM were also removed. Tag directories were then generated for each sample using HOMER v4.4. For the TFE3 ChIP, the HOMER program getDifferentialPeaksReplicates.pl (v4.11) was used twice for each genotype group (control, LiFKO, control+1c, LiFKO+1c) to call peaks over either (1) each genotype's respective input sample or (2) the 1 TFE3 ChIP samples done in the *Tfe3* KO genotype. For the HA ChIP, getDifferentialPeaksReplicates.pl was used twice for each genotype group (control+1c, LiFKO+1c) to call peaks over either (1) each genotype's respective input sample or (2) the HA ChIP samples done in control or LiFKO mice not injected with HA-nSREBP-1c virus (non-HA control). The option -all was used on this program to output all peaks called, and default settings were used (at least a fold-change of 4 and FDR of 0.001). The 2 peaksets generated for each genotype group were then merged using mergePeaks (HOMER, v4.11), and overlapping peaks were designated as the final peakset for each genotype. To determine differentially regulated peaks in one genotype vs. a second genotype (i.e,. HA peaks in LiFKO+1c vs. control+1c livers as in Fig. S10B, or TFE3 peaks in LiFKO+1c vs. LiFKO livers, as in Fig. S10C-D), getDifferentialPeaksReplicates.pl was used using the 1st genotype as the -t (target) option and the 2nd genotype as the -b (background) option. The 1st genotype's input sample was used as the -i (input) option. Using getDifferentialPeaksReplicates.pl, the 1st genotype's peaks were first called over input (using default settings: at least a fold-change of 4 and FDR of 0.001) as above, followed by differential expression analysis between the 1st and 2nd genotypes, to determine differentially regulated peaks with at least a 2-fold change and FDR of 5% (the default settings). Enriched motifs were found in the above peaksets via findMotifsGenome.pl (HOMER, v4.11). Motif HTML files were cleaned up using the Beautiful Soup python library, for visualization. Enriched pathways were found in the peaksets via findGO.pl (HOMER, v4.11); specifically the most enriched Reactome pathways were depicted in this paper. bedGraph and bigWig files were generated via HOMER makeUCSCfile and bedGraphtoBigWig, and they were normalized to 1e7 reads per sample and input control. WashU Epigenome Browser was used for visualization of these bigWig files. To determine TFE3 enrichment near the TFE3 peakset determined in the control genotype, the HOMER program annotatePeaks.pl (v4.11) was used on bedGraph files, using the -hist (histogram) option to determine enrichment in 10 basepair (bp) bins within 1000 bp of the TFE3 peaks. This method was also used to determine HA-nSREBP-1c enrichment near the HA peakset determined in the control+1c condition. To determine TFE3 enrichment at HA-nSREBP-1c peaks under FPC diet conditions, the HA peakset generated for the control+1c mice was annotated using HOMER annotatepeaks.pl. Then, using the -hist option on annotatePeaks.pl again, TFE3 enrichment (in 10 bp bins) was determined on (1) all nSREBP-1c peaks, (2) just peaks within 5kb of a TSS, and (3) peaks within 5kb of TSS's of de novo lipogenesis genes (specifically, *Fasn*, *Mlxipl*, *Srebf1*, *Scd1*, *Acaca*, *Acacb*, *Acly*, *Acss2*); enrichment was calculated within 1000 bp from peak center, using TFE3 bedGraph files. TFE3 enrichment (within 1000 bp from peak center) on all nSREBP-1c peaks was also determined with deepTools v3.3.0 using the computeMatrix (reference-point mode) and plotHeatmap commands on TFE3 bigwig files.

All other quantification, statistical analysis, and figure creation

Mice were randomized to experimental groups. Data are represented as mean +/- SEM for biological replicates, unless otherwise stated. Researchers were not blinded to experimental groups. Samples sizes were not pre-determined. For comparisons between control, LiFKO, *Tfe3* KO, and DKO (or control, LiFKO, and DKO) genotypes under the same dietary condition, 1-way ANOVA with Tukey's multiple comparison's test was used. The same test was used when comparing genotypes in the NASH reversal experiment, comparing non-injected, control, and LiFKO mice. To compare body weights over time, and to analyze GTT, we used repeated measures 2-way ANOVA or mixed-effects ANOVA, with either Tukey's multiple comparisons test for 3+ genotypes or Sidak's multiple comparisons test for 2 genotypes. For energy expenditure, food consumption, water consumption, and energy balance measured with CLAMS, ANCOVA with covariate for lean mass was performed as stated above. To compare numbers of mice with fibrosis (only stage 1A was observed of all fibrosis stages) or without fibrosis via blinded histological evaluation, Fisher's exact test was performed. For all other analyses, student's two-tailed t-test was used between the genotypes indicated. Significance was determined as $p<0.05$. Python 3 was used for ANCOVA analysis; R was used for Fisher's exact test; all other statistical analyses and graphing was done using Graphpad Prism 8. Next generation sequencing data is available through the GEO accession number GSE160292. Data figures were created using Prism 8 and R. Adobe Illustrator was used for figure formatting. ChIP-seq peaks were visualized with WashU Epigenome Browser. Deeptools was also used for ChIP-seq visualization (Fig. S10A). Morpheus was used for heatmaps. The Print Page Summary figure and schematics of mice and syringes (Fig. 1C, 4E, 4F, 5F, 6F, and S8C) were created with BioRender.com

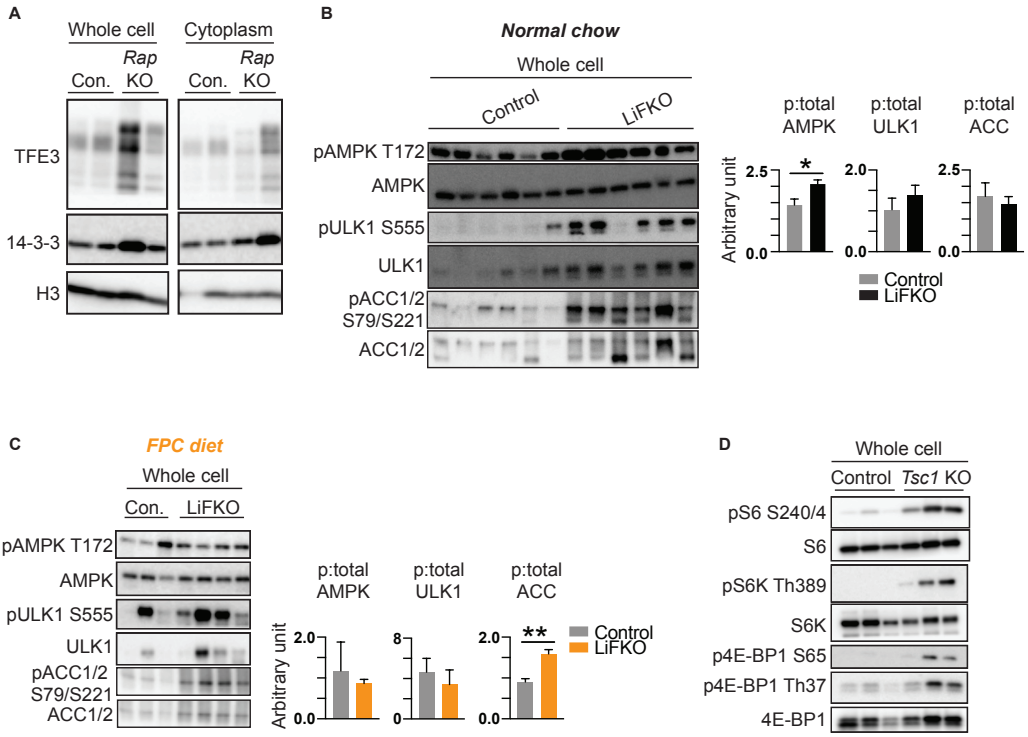
A
Whole cell
Cytoplasm
Rap
Con.
KO
TFE3
14-3-3
H3
B
Normal chow
Whole cell
Control
LiFKO
pAMPK T172
AMPK
pULK1 S555
ULK1
pACC1/2
S79/S221
ACC1/2
p:total
AMPK
p:total
ULK1
p:total
ACC
Arbitrary unit
2.5
0.0
2.0
*
Control
LiFKO
C
FPC diet
Whole cell
Con.
LiFKO
pAMPK T172
AMPK
pULK1 S555
ULK1
pACC1/2
S79/S221
ACC1/2
p:total
AMPK
p:total
ULK1
p:total
ACC
Arbitrary unit
2.0
0.0
8
**
Control
LiFKO
D
Whole cell
Control
Tsc1 KO
pS6 S240/4
S6
pS6K Th389
S6K
p4E-BP1 S65
p4E-BP1 Th37
4E-BP1

Fig. S1. FLCN in hepatocytes selectively promotes mTORC1-mediated phosphorylation and cytoplasmic sequestration of TFE3 in mouse liver, without affecting canonical mTORC1 or AMPK signaling

(A) Control and *Raptor* liver KO mice on normal chow were euthanized after an overnight fast followed by 4 hours of refeeding. Subcellular fractionation was performed as in Fig. 1E. Immunoblotting was done on cytoplasmic and whole cell fractions, with 14-3-3 as a loading control. Quantification is depicted in Fig. 1F.

(B-C) Control and LiFKO mice were fed either (B) normal chow or (C) 7-8 days of FPC diet (TD190142 and sugar water) and euthanized after an overnight fast followed by a ~4 hour refeeding period. Livers were then subjected to immunoblotting and quantification of AMPK signaling, including phosphorylated AMPK, ULK1, and ACC1/2 (of note, the top ACC band was quantified). HSP90 (Fig. 1D) or beta actin (Fig. 1H) were loading controls. * < p=0.05, ** < p=0.01. Student's two-tailed t-test were used to assess differences between control and LiFKO genotypes. Data are depicted as mean +/- SEM.

(D) Whole cell lysates were examined for canonical mTORC1 signaling from livers of control and liver *Tsc1* KO mice, euthanized ad lib. 14-3-3 (Fig. 1J) was a loading control.

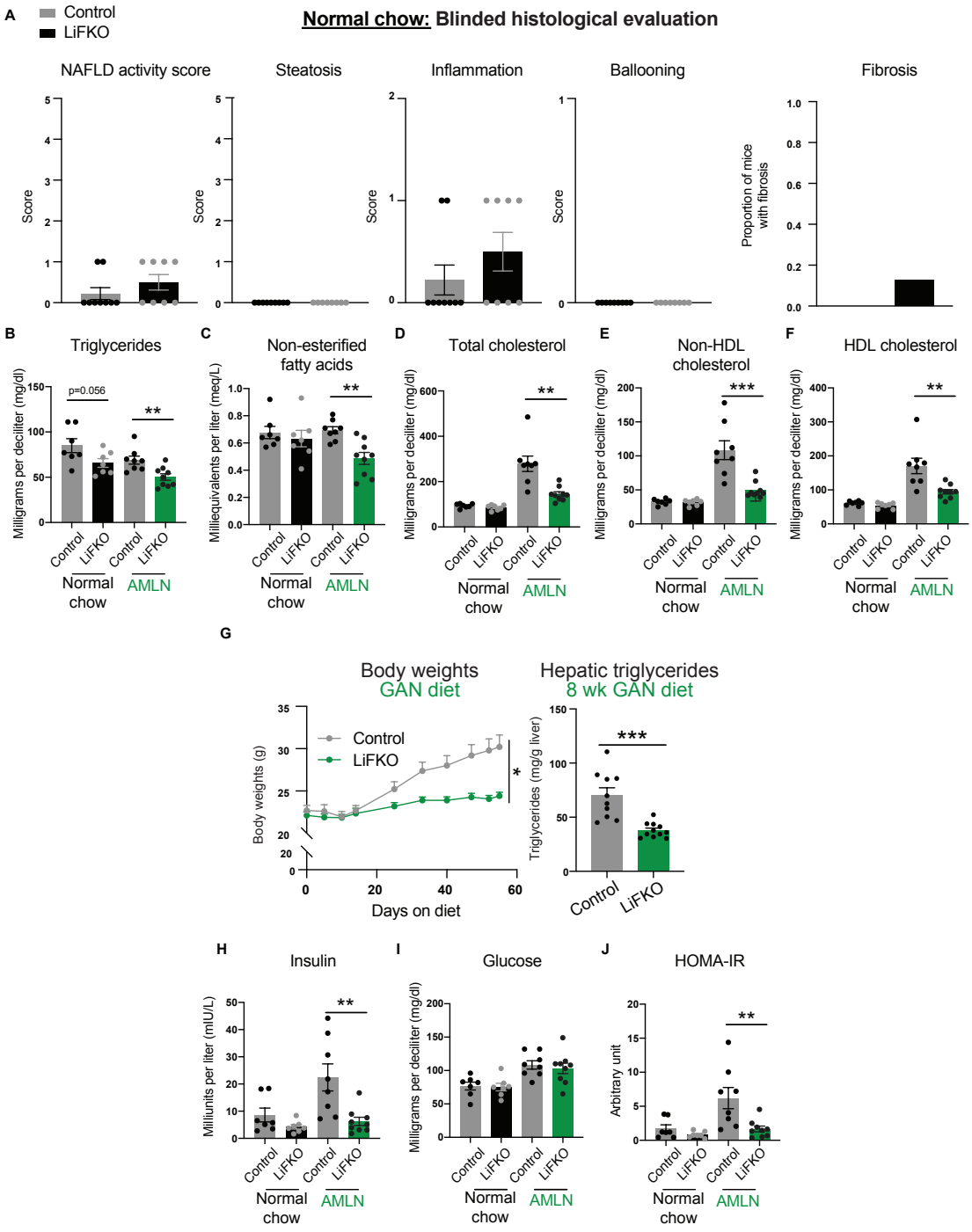
A
Control
LiFKO
Normal chow: Blinded histological evaluation
NAFLD activity score
Steatosis
Inflammation
Ballooning
Fibrosis
Score
Proportion of mice with fibrosis
B
Triglycerides
Milligrams per deciliter (mg/dl)
p=0.056
**
C
Non-esterified fatty acids
Milliequivalents per liter (meq/L)
**
D
Total cholesterol
Milligrams per deciliter (mg/dl)
**
E
Non-HDL cholesterol
Milligrams per deciliter (mg/dl)
***
F
HDL cholesterol
Milligrams per deciliter (mg/dl)
**
Control
LiFKO
Normal chow
AMLN
G
Body weights
GAN diet
Body weights (g)
Days on diet
*
Hepatic triglycerides
8 wk GAN diet
Triglycerides (mg/g liver)
***
H
Insulin
Milliunits per liter (mIU/L)
**
I
Glucose
Milligrams per deciliter (mg/dl)
J
HOMA-IR
Arbitrary unit
**

Fig. S2. FLCN deletion in the liver protects against NAFLD and many aspects of metabolic syndrome

(A) Blinded histological evaluation of liver H&E slides (for NAFLD activity score, steatosis, inflammation, and ballooning) and Sirius Red slides (for fibrosis; livers either exhibited no fibrosis or fibrosis stage 1A), from mice fed 16-17 weeks of normal chow and fasted for 4-6 hours (n=8-9)

(B-F) Plasma measurements of (B) triglycerides, (C) non-esterified fatty acids, (D) total cholesterol, (E) non-HDL cholesterol, and (F) HDL cholesterol in control and LiFKO mice fed either 17-18.5 weeks of normal chow (n=7) or AMLN diet (n=8-9), and fasted for 4-6 hours.

(G) Control and LiFKO mice (n=10-11) were fed 8 weeks of GAN diet then euthanized after a 5-hour fast. Weekly body weights were measured during the experiment, and hepatic triglycerides were quantified after euthanasia.

(H-J) Plasma insulin (H) and blood glucose (I) measurements of control and LiFKO mice fed either 16-17 weeks of normal chow (n=7) or AMLN diet (n=8-9), and fasted overnight. (J) Homeostatic model assessment of insulin resistance (HOMA-IR) was calculated by multiplying the insulin values by glucose values and dividing by 405.

* < p=0.05, ** < p=0.01, *** < p=0.001. Fisher's exact test was used to compare number of livers with fibrosis between the genotypes. Mixed effects analysis with multiple comparisons test was used to compare control and LiFKO body weights, and the statistical value for the last time point is indicated. Student's two-tailed t-test was used to compare control and LiFKO genotypes in all other analyses. Data are depicted as mean +/- SEM.

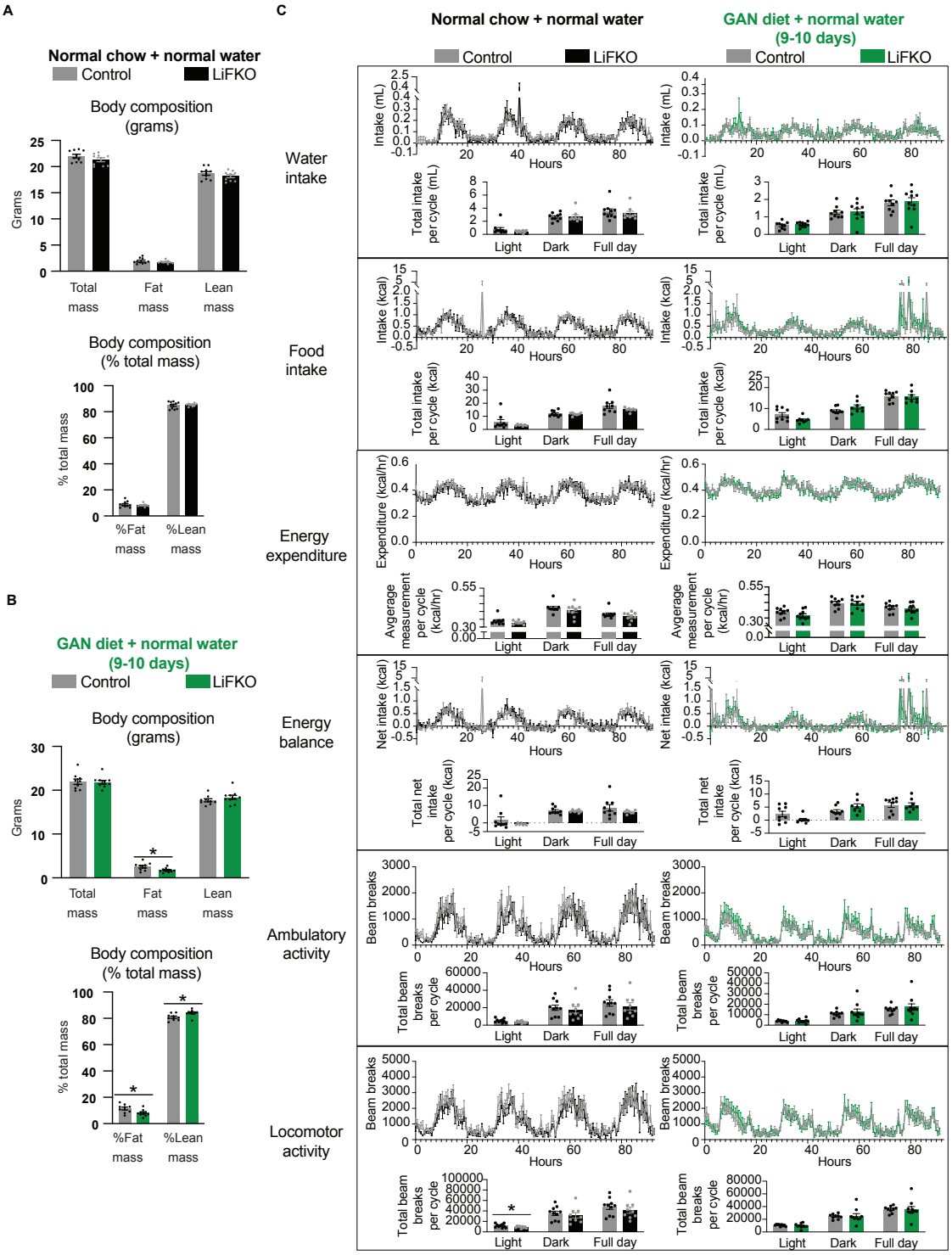
A
Normal chow + normal water
Control
LiFKO
Body composition (grams)
Grams
Total mass
Fat mass
Lean mass
Body composition (% total mass)
% total mass
%Fat mass
%Lean mass
B
GAN diet + normal water (9-10 days)
Control
LiFKO
Body composition (grams)
Grams
Total mass
Fat mass
Lean mass
Body composition (% total mass)
% total mass
%Fat mass
%Lean mass
C
Normal chow + normal water
GAN diet + normal water (9-10 days)
Control
LiFKO
Water intake
Food intake
Energy expenditure
Energy balance
Ambulatory activity
Locomotor activity
Intake (mL)
Intake (kcal)
Expenditure (kcal/hr)
Net intake (kcal)
Beam breaks
Hours
Total intake per cycle (mL)
Total intake per cycle (kcal)
Avgerage measurement per cycle (kcal/hr)
Total net intake per cycle (kcal)
Total beam breaks per cycle
Light
Dark
Full day

Fig. S3. FLCN deletion in the liver does not affect whole body energy metabolism in normal chow or GAN diet

Control and LiFKO mice (n=9-10) were fed either (A, C) normal chow or (B, C) 9-10 days of GAN diet.

(A-B) EchoMRI was performed to measure fat and lean mass composition. Student's two-tailed t-test was used for analysis.

(C) CLAMS was performed to measure food consumption, water consumption, energy expenditure, energy balance, ambulatory activity, and locomotor activity at 40-minute intervals. The average interval energy expenditure was then calculated over all of the light cycles of the study, all of the dark cycles, or the entire course of the study (full day). For the rest of the parameters studied, values were summed either for all of the light cycles, all of the dark cycles, or the entire study overall (full day). The values were then divided by the number of light cycles, dark cycles, and days of the study, respectively. Control and LiFKO mice were compared using ANCOVA with covariate for lean mass on these "per cycle" average values, for water consumption, food consumption, energy expenditure, and energy balance. Student's two-tailed t-test was used for activity measurements.

* < p=0.05. Data are depicted as mean +/- SEM.

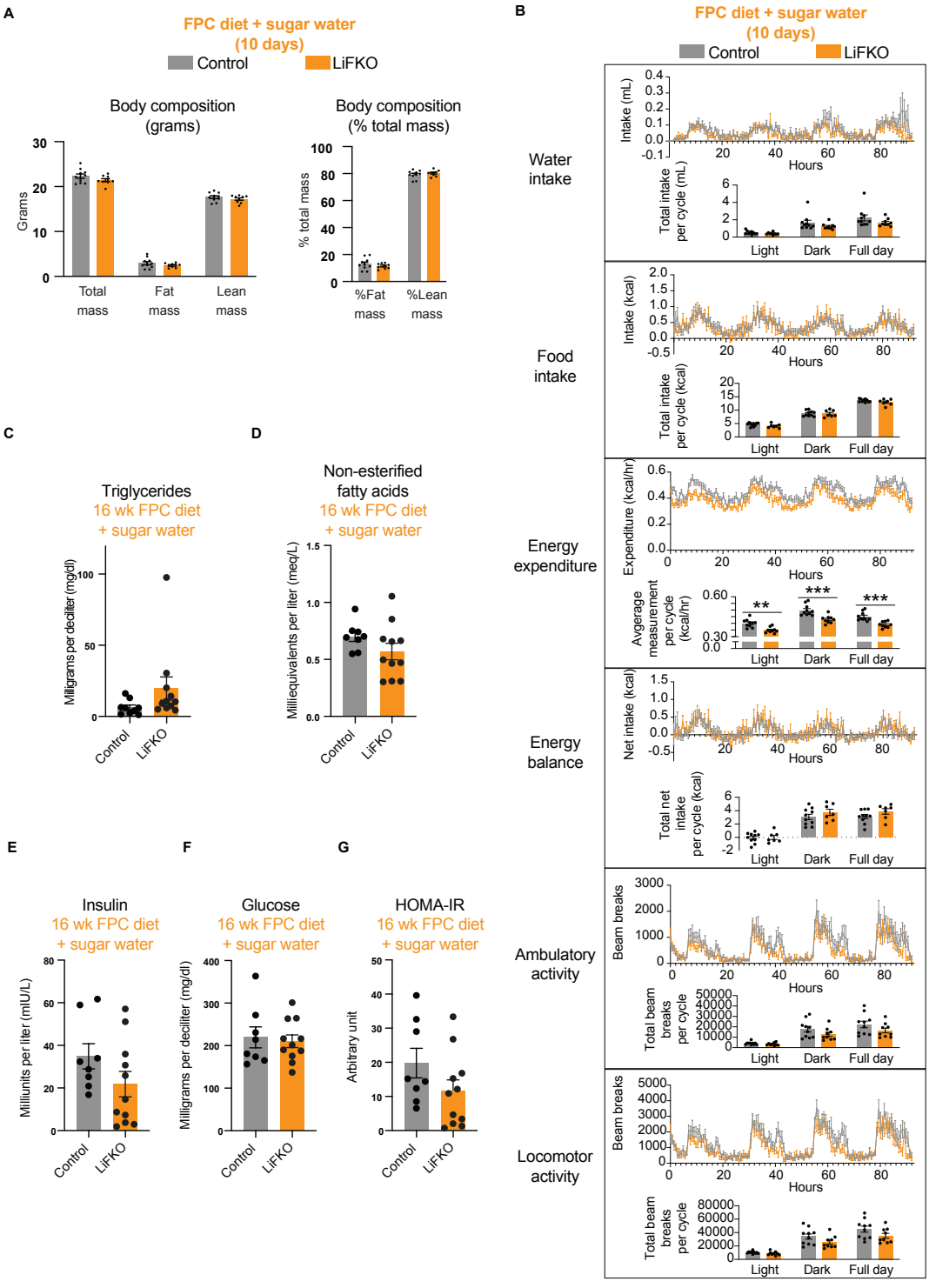
A
FPC diet + sugar water
(10 days)
Control
LiFKO
Body composition
(grams)
Grams
Total mass
Fat mass
Lean mass
Body composition
(% total mass)
% total mass
%Fat mass
%Lean mass
B
FPC diet + sugar water
(10 days)
Control
LiFKO
Water intake
Intake (mL)
Hours
Total intake per cycle (mL)
Light
Dark
Full day
Food intake
Intake (kcal)
Total intake per cycle (kcal)
Energy expenditure
Expenditure (kcal/hr)
Avgerage measurement per cycle (kcal/hr)
Energy balance
Net intake (kcal)
Total net intake per cycle (kcal)
Ambulatory activity
Beam breaks
Total beam breaks per cycle
Locomotor activity
C
Triglycerides
16 wk FPC diet
+ sugar water
Milligrams per deciliter (mg/dl)
D
Non-esterified fatty acids
16 wk FPC diet
+ sugar water
Milliequivalents per liter (meq/L)
E
Insulin
16 wk FPC diet
+ sugar water
Milliunits per liter (mIU/L)
F
Glucose
16 wk FPC diet
+ sugar water
Milligrams per deciliter (mg/dl)
G
HOMA-IR
16 wk FPC diet
+ sugar water
Arbitrary unit

Fig. S4. FLCN deletion in the liver does not protect against metabolic syndrome in FPC diet conditions, and largely does not affect whole body energy metabolism
(A-B) Control and LiFKO mice (n=9-10) were fed 10 days of FPC diet (TD190142) and sugar water.
(A) EchoMRI was performed to measure fat and lean mass composition. Student's two-tailed t-test was used for analysis.
(B) CLAMS was performed to measure food consumption, water consumption, energy expenditure, energy balance, ambulatory activity, and locomotor activity at 40-minute intervals. The average interval energy expenditure was then calculated over all of the light cycles of the study, all of the dark cycles, or the entire course of the study (full day). For the rest of the parameters studied, values were summed either for all of the light cycles, all of the dark cycles, or the entire study overall (full day). The values were then divided by the number of light cycles, dark cycles, and days of the study, respectively. Control and LiFKO mice were compared using ANCOVA with covariate for lean mass on these "per cycle" average values, for water consumption, food consumption, energy expenditure, and energy balance. Student's two-tailed t-test was used for activity measurements.
(C-G) Plasma measurements of (C) triglycerides, (D) non-esterified fatty acids, (E) insulin, and (F) glucose in control and LiFKO mice (n=8-11) fed 16 weeks of FPC diet regimen (TD160785 and sugar water) then fasted 4-6 hours (food removed but not sugar water). (G) HOMA-IR was calculated by multiplying the insulin values by the glucose values and dividing by 405. Student's two-tailed t-test was used for analysis.
** < p=0.01, *** < p=0.001. Data are depicted as mean +/- SEM.

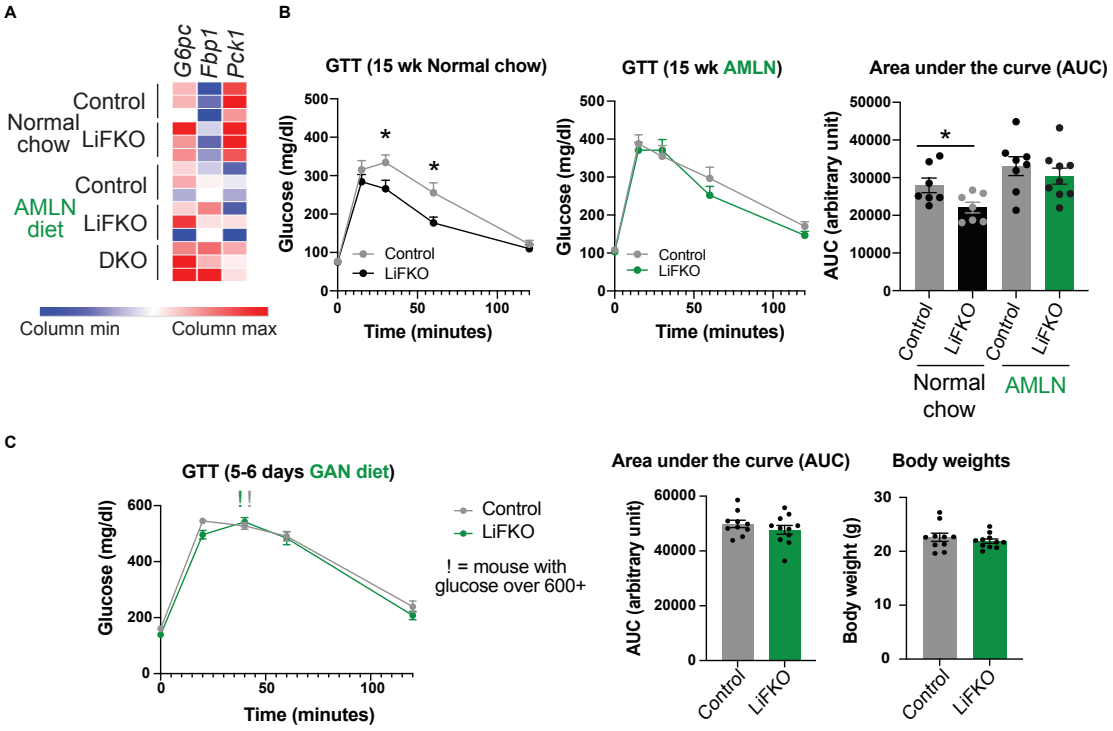
A
G6pc
Fbp1
Pck1
Control
Normal chow
LiFKO
Control
AMLN diet
LiFKO
DKO
Column min
Column max
B
GTT (15 wk Normal chow)
Glucose (mg/dl)
Time (minutes)
Control
LiFKO
GTT (15 wk AMLN)
Area under the curve (AUC)
AUC (arbitrary unit)
Normal chow
AMLN
C
GTT (5-6 days GAN diet)
! = mouse with glucose over 600+
Area under the curve (AUC)
Body weights
Body weight (g)

Fig. S5. FLCN deletion in the liver does not increase gluconeogenesis genes or glucose intolerance

(A) RNA-sequencing was performed on the livers of n=3 control, LiFKO, and DKO mice on 17-18.5 weeks normal chow or AMLN diet. The normalized expression values of gluconeogenesis genes were visualized via heatmap for all genotypes.

(B) Control and LiFKO mice fed 16 weeks of normal chow (n=7) or AMLN diet (n=8-9) were fasted overnight then gavaged with 2g/kg of D-glucose, followed by serial blood glucose measurements (a glucose tolerance test, i.e. GTT). GTT data was plotted and area under the curve (AUC) was calculated to assess glucose tolerance.

(C) Control and LiFKO mice fed 5-6 days of GAN diet (n=10-11) were fasted for 5 hours then gavaged with 2g/kg of D-glucose, followed by serial blood glucose measurements. AUC was calculated to assess glucose tolerance.

* < p=0.05. 2-way repeated measures ANOVA with multiple comparison's test was used to compare serial blood glucose measurements between control and LiFKO genotypes. AUC was analyzed with Student's two-tailed t-test. Data are depicted as mean +/- SEM.

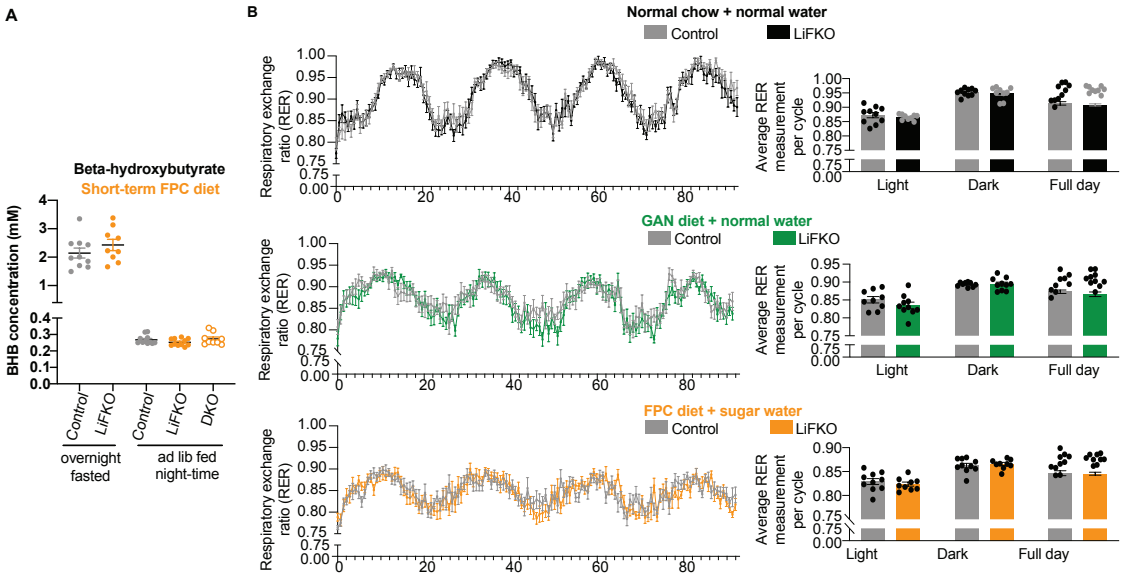
A
Beta-hydroxybutyrate
Short-term FPC diet
BHB concentration (mM)
Control
LiFKO
Control
LiFKO
DKO
overnight fasted
ad lib fed night-time
B
Normal chow + normal water
Control
LiFKO
Respiratory exchange ratio (RER)
Average RER measurement per cycle
Light
Dark
Full day
GAN diet + normal water
FPC diet + sugar water

Fig. S6. FLCN deletion in the liver does not increase functional fatty acid oxidation
(A) Plasma beta-hydroxybutyrate was measured in mice fed 2.5 weeks of FPC diet regimen (TD190142 and sugar water) and fasted overnight (n=9-10) or mice treated with 9 days of FPC diet regimen (TD190142 and sugar water) and ad lib fed during the night time (n=9-11). Control and LiFKO mice that were fasted were compared using Student's two-tailed t-test. Control, LiFKO, and DKO mice that were ad lib fed were compared using 1-way ANOVA with Tukey's multiple comparisons test.
(B) Respiratory exchange ratios from the same mice as in Fig. S3-S4. The average interval respiratory exchange ratio was calculated over all of the light cycles of the study, all of the dark cycles, or the entire course of the study (full day). Control and LiFKO mice were compared using Student's two-tailed t-test on these "per cycle" average values.
Data are depicted as mean +/- SEM.

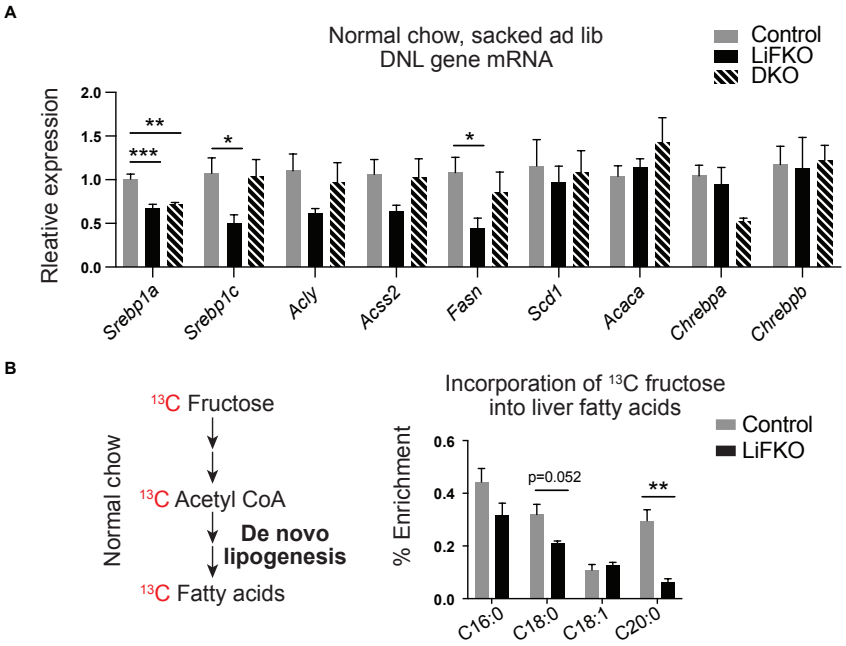
A
Normal chow, sacked ad lib
DNL gene mRNA
Control
LiFKO
DKO
Rleative expression
2.0
1.5
1.0
0.5
0.0
**
***
*
*
Srebp1a
Srebp1c
Acly
Acss2
Fasn
Scd1
Acaca
Chrebpa
Chrebpb
B
Normal chow
13C Fructose
13C Acetyl CoA
De novo lipogenesis
13C Fatty acids
Incorporation of 13C fructose into liver fatty acids
Control
LiFKO
% Enrichment
0.6
0.4
0.2
0.0
p=0.052
**
C16:0
C18:0
C18:1
C20:0

Fig. S7. Hepatic FLCN deletion inhibits de novo lipogenesis activity on normal chow mildly

(A) qRT-PCR of de novo lipogenesis genes in livers of control, LiFKO, and DKO mice fed normal chow and euthanized ad lib (n=5-6). 1-way ANOVA with Tukey's multiple comparisons test was used to assess differences between control, LiFKO, and DKO genotypes.

(B) Control and LiFKO mice (n=3) fed normal chow were fasted from 9am-7pm, refed for 2 hours, and gavaged a bolus of ^{13}C-fructose and ^{12}C-glucose. The mice were then fed overnight and euthanized the next morning. LC-MS was performed to examine the amount of ^{13}C label incorporation into hepatic fatty acids. Student's two-tailed t-test was used to compare genotypes.

* < p=0.05, ** < p=0.01. Data are depicted as mean +/- SEM.

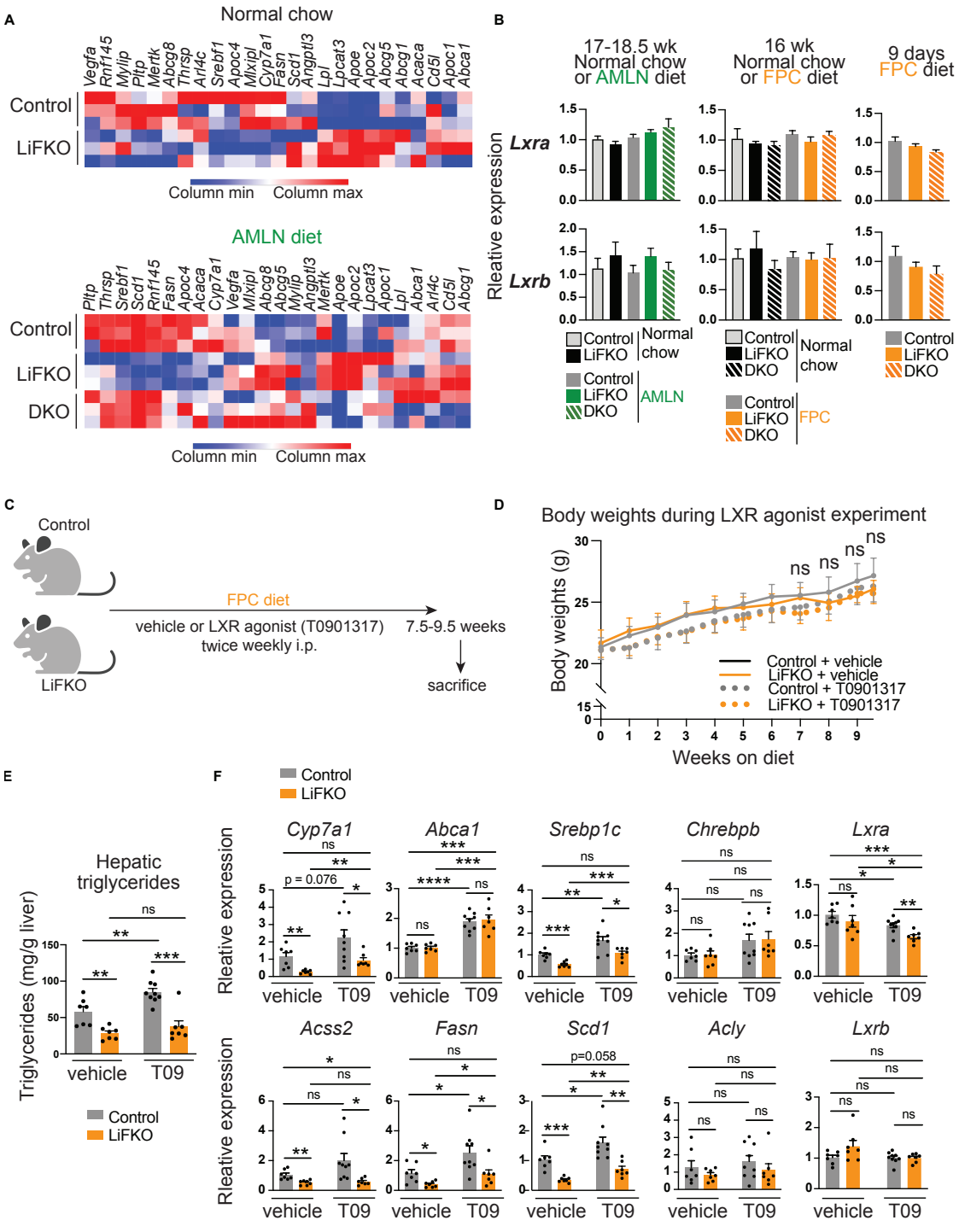
A
Normal chow
Vegfa Rnf145 Mylip Pltp Mertk Abcg8 Thrsp Arl4c Srebf1 Apoc4 Mlxipl Cyp7a1 Fasn Scd1 Angptl3 Lpl Lpcat3 Apoe Apoc2 Abcg5 Abcg1 Acaca Cd5l Apoc1 Abca1
Control
LiFKO
Column min Column max
AMLN diet
Pltp Thrsp Srebf1 Scd1 Rnf145 Fasn Apoc4 Acaca Cyp7a1 Vegfa Mlxipl Abcg8 Abcg5 Mylip Angptl3 Mertk Apoe Apoc2 Lpcat3 Apoc1 Lpl Abca1 Arl4c Cd5l Abcg1
Control
LiFKO
DKO
Column min Column max
B
17-18.5 wk Normal chow or AMLN diet
16 wk Normal chow or FPC diet
9 days FPC diet
Rleative expression
Lxra
Lxrb
Control LiFKO Normal chow
Control LiFKO DKO Normal chow
Control LiFKO DKO AMLN
Control LiFKO DKO FPC
Control LiFKO DKO
C
Control
LiFKO
FPC diet
vehicle or LXR agonist (T0901317) twice weekly i.p.
7.5-9.5 weeks
sacrifice
D
Body weights during LXR agonist experiment
Body weights (g)
Weeks on diet
Control + vehicle
LiFKO + vehicle
Control + T0901317
LiFKO + T0901317
ns
E
Hepatic triglycerides
Triglycerides (mg/g liver)
vehicle T09
Control
LiFKO
F
Control
LiFKO
Rleative expression
Cyp7a1 Abca1 Srebp1c Chrebpb Lxra
Acss2 Fasn Scd1 Acly Lxrb
p = 0.076
p=0.058
vehicle T09

Fig. S8. TFE3 acts downstream of LXR to suppress DNL
(A) RNA-sequencing was performed on the livers of n=3 control, LiFKO, and DKO mice on 17-18.5 weeks of normal chow or AMLN diet. The normalized expression values of LXR target genes were visualized via heatmap for all genotypes.
(B) mRNA expression of LXR levels in livers of control, LiFKO, and DKO mice fed (left) normal chow (n=7) or 17-18.5 weeks of AMLN diet (B; n=3-9); (middle) normal chow (n=3) or 16 weeks of FPC diet regimen (TD160785 and sugar water; n=7-11); or (right) 9 days of FPC diet regimen and euthanized at 10 pm ad lib (TD190142 and sugar water; n=7-9). For normal chow controls for the AMLN diet experiment, Student's two-tailed t-test was used to compare control and LiFKO. In all other conditions, 1-way ANOVA with Tukey's multiple comparisons test was used.
(C-F) Control and LiFKO mice (n=7-9) were fed ~7.5-9.5 weeks of FPC diet regimen (TD190142 and sugar water) in conjunction with twice weekly intraperitoneal injections of vehicle or LXR agonist (T0901317). The mice were then euthanized ad lib in the morning. Student's two-tailed t-test was used for analysis.
(C) Schematic of LXR agonist rescue experiment.
(D) Body weights of the mice. Mixed effects analysis with multiple comparisons test was used to compare control and LiFKO mice. Statistical analyses shown for weeks 7, 8, 9, and 9.5.
(E) Measurement of liver triglycerides in control and LiFKO mice treated with either vehicle or T0901317.
(F) qRT-PCR of core de novo lipogenesis genes, LXR target genes, and LXR levels in livers of these mice.
* < p=0.05, ** < p=0.01, *** < p=0.001, **** < p=0.0001, ***** < p=0.00001. Data are depicted as mean +/- SEM.

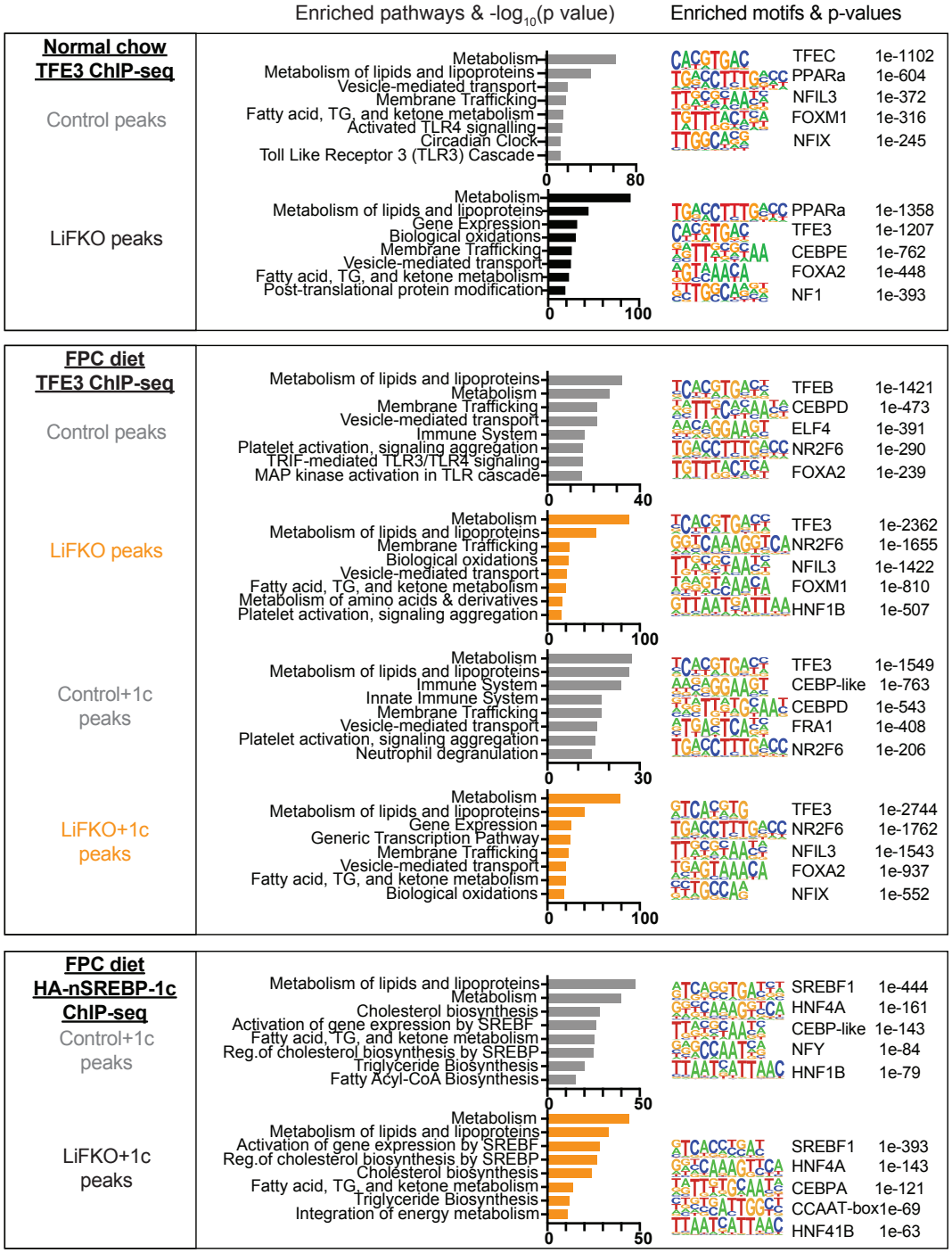
Enriched pathways & -log10(p value)
Enriched motifs & p-values
Normal chow
TFE3 ChIP-seq
Control peaks
Metabolism
Metabolism of lipids and lipoproteins
Vesicle-mediated transport
Membrane Trafficking
Fatty acid, TG, and ketone metabolism
Activated TLR4 signalling
Circadian Clock
Toll Like Receptor 3 (TLR3) Cascade
0
80
TFEC 1e-1102
PPARa 1e-604
NFIL3 1e-372
FOXM1 1e-316
NFIX 1e-245
LiFKO peaks
Metabolism
Metabolism of lipids and lipoproteins
Gene Expression
Biological oxidations
Membrane Trafficking
Vesicle-mediated transport
Fatty acid, TG, and ketone metabolism
Post-translational protein modification
0
100
PPARa 1e-1358
TFE3 1e-1207
CEBPE 1e-762
FOXA2 1e-448
NF1 1e-393
FPC diet
TFE3 ChIP-seq
Control peaks
Metabolism of lipids and lipoproteins
Metabolism
Membrane Trafficking
Vesicle-mediated transport
Immune System
Platelet activation, signaling aggregation
TRIF-mediated TLR3/TLR4 signaling
MAP kinase activation in TLR cascade
0
40
TFEB 1e-1421
CEBPD 1e-473
ELF4 1e-391
NR2F6 1e-290
FOXA2 1e-239
LiFKO peaks
Metabolism
Metabolism of lipids and lipoproteins
Membrane Trafficking
Biological oxidations
Vesicle-mediated transport
Fatty acid, TG, and ketone metabolism
Metabolism of amino acids & derivatives
Platelet activation, signaling aggregation
0
100
TFE3 1e-2362
NR2F6 1e-1655
NFIL3 1e-1422
FOXM1 1e-810
HNF1B 1e-507
Control+1c peaks
Metabolism
Metabolism of lipids and lipoproteins
Immune System
Innate Immune System
Membrane Trafficking
Vesicle-mediated transport
Platelet activation, signaling aggregation
Neutrophil degranulation
0
30
TFE3 1e-1549
CEBP-like 1e-763
CEBPD 1e-543
FRA1 1e-408
NR2F6 1e-206
LiFKO+1c peaks
Metabolism
Metabolism of lipids and lipoproteins
Gene Expression
Generic Transcription Pathway
Membrane Trafficking
Vesicle-mediated transport
Fatty acid, TG, and ketone metabolism
Biological oxidations
0
100
TFE3 1e-2744
NR2F6 1e-1762
NFIL3 1e-1543
FOXA2 1e-937
NFIX 1e-552
FPC diet
HA-nSREBP-1c
ChIP-seq
Control+1c peaks
Metabolism of lipids and lipoproteins
Metabolism
Cholesterol biosynthesis
Activation of gene expression by SREBF
Fatty acid, TG, and ketone metabolism
Reg.of cholesterol biosynthesis by SREBP
Triglyceride Biosynthesis
Fatty Acyl-CoA Biosynthesis
0
50
SREBF1 1e-444
HNF4A 1e-161
CEBP-like 1e-143
NFY 1e-84
HNF1B 1e-79
LiFKO+1c peaks
Metabolism
Metabolism of lipids and lipoproteins
Activation of gene expression by SREBF
Reg.of cholesterol biosynthesis by SREBP
Cholesterol biosynthesis
Fatty acid, TG, and ketone metabolism
Triglyceride Biosynthesis
Integration of energy metabolism
0
50
SREBF1 1e-393
HNF4A 1e-143
CEBPA 1e-121
CCAAT-box 1e-69
HNF41B 1e-63

Fig. S9. TFE3 and HA-nSREBP-1c ChIP-seq unbiased pathway and motif analysis
(Top) TFE3 ChIP-seq was performed on livers of control (n=4), LiFKO (n=4), and *Tfe3* KO (n=2) mice fed normal chow and euthanized ad lib in the morning/afternoon. Peaks were then called in the control and LiFKO conditions (over input and *Tfe3* KO). (Middle and bottom) Using the liver samples from the nSREBP-1c rescue experiment (done in FPC regimen conditions; TD190142 and sugar water) described in Fig. 5F, both (middle) a TFE3 ChIP-seq and (bottom) an HA-nSREBP-1c ChIP-seq was performed. For the TFE3 ChIP-seq, peaks were called in each genotype tested: Control, LiFKO, Control+1c, LiFKO+1c (over input and *Tfe3* KO). For the HA-nSREBP-1c ChIP-seq, peaks were called in the Control+1c and LiFKO+1c genotypes (over input control and livers not injected with HA-nSREBP-1c). Reactome pathway analysis and unbiased motif discovery was then performed on all peak sets via Homer.

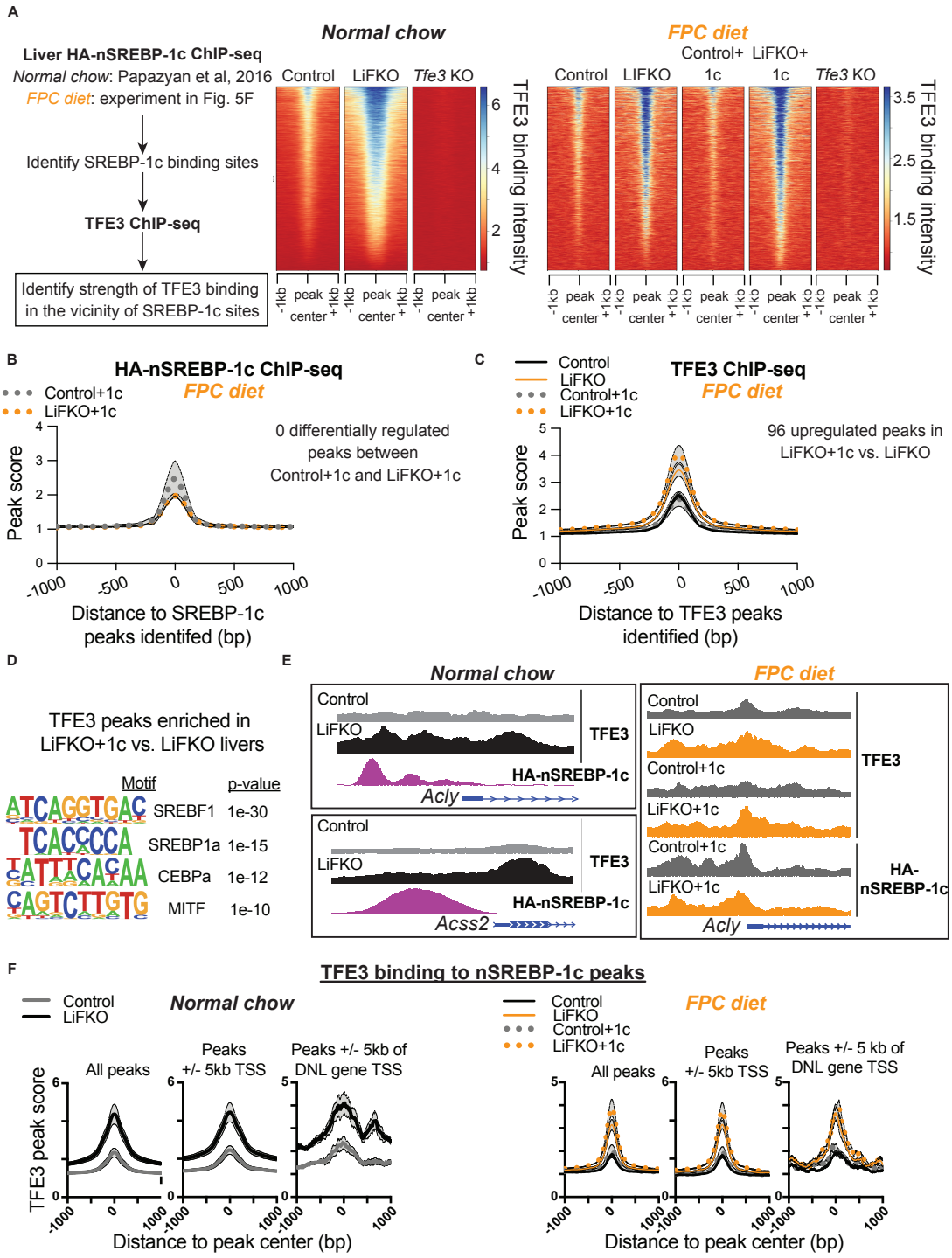
A
Normal chow
FPC diet
Liver HA-nSREBP-1c ChIP-seq
Normal chow: Papazyan et al, 2016
FPC diet: experiment in Fig. 5F
Identify SREBP-1c binding sites
TFE3 ChIP-seq
Identify strength of TFE3 binding in the vicinity of SREBP-1c sites
Control
LiFKO
Tfe3 KO
Control+
1c
LiFKO+
TFE3 binding intensity
-1kb
peak center
+1kb
B
HA-nSREBP-1c ChIP-seq
FPC diet
Control+1c
LiFKO+1c
0 differentially regulated peaks between Control+1c and LiFKO+1c
Peak score
Distance to SREBP-1c peaks identifed (bp)
C
TFE3 ChIP-seq
FPC diet
Control
LiFKO
Control+1c
LiFKO+1c
96 upregulated peaks in LiFKO+1c vs. LiFKO
Peak score
Distance to TFE3 peaks identified (bp)
D
TFE3 peaks enriched in LiFKO+1c vs. LiFKO livers
Motif
p-value
SREBF1 1e-30
SREBP1a 1e-15
CEBPa 1e-12
MITF 1e-10
E
Normal chow
FPC diet
Control
LiFKO
Control+1c
LiFKO+1c
TFE3
HA-nSREBP-1c
HA-nSREBP-1c
Acly
Acss2
F
TFE3 binding to nSREBP-1c peaks
Control
LiFKO
Control+1c
LiFKO+1c
Normal chow
FPC diet
All peaks
Peaks +/- 5kb TSS
Peaks +/- 5kb of DNL gene TSS
TFE3 peak score
Distance to peak center (bp)

Fig. S10. TFE3 synergistically occupies chromatin in close proximity to SREBP-1c genome-wide

(A) Genome-wide SREBP-1c binding sites were identified from either publicly available data (GSM2287950; for normal chow) or from an HA-nSREBP-1c ChIP-seq performed in control+1c mice from Fig. 5F (for FPC diet; TD190142 with sugar water). TFE3 ChIP-seq data was then used to map TFE3 binding to these SREBP-1c sites. Left: schematic. Middle and right: binding of TFE3 on or near SREBP-1c binding sites in livers from control, LiFKO, and *Tfe3* KO mice maintained on normal chow (middle) or on FPC diet (TD190142 with sugar water) and co-infected where indicated with AAV8-ApoE/AAT-HA-nSREBP-1c ("1c"; right). Depicted are binding intensity measurements from 1 representative sample per genotype.

(B) (left) Binding by HA-nSREBP-1c, in livers from n=3 control and LiFKO mice infected with AAV8-ApoE/AAT-HA-nSREBP-1c ("1c") and maintained on FPC diet, near HA peaks identified in the control+1c condition. Data are depicted as mean +/- SEM. (right) Differentially expressed peaks between control+1c and LiFKO+1c livers, calculated with Homer getDifferentialPeaksReplicates, using an FDR cut-off of 5% and a fold-change cut-off of 2.

(C) (left) Binding by TFE3, in livers from n=3 control and LiFKO mice infected with control virus or AAV8-ApoE/AAT-HA-nSREBP-1c ("1c") and maintained on FPC diet, near TFE3 peaks identified in the control condition. (right) Differentially expressed peaks between LiFKO+1c vs. LiFKO livers, calculated with Homer getDifferentialPeaksReplicates, using an FDR cut-off of 5% and a fold-change cut-off of 2.

(D) Unbiased motif discovery of TFE3 binding sites enriched in livers from LiFKO mice infected with AAV8-HA-nSREBP-1c ("1c"), compared with LiFKO mice infected with a control virus.

(E) Visualization of binding by TFE3 or HA-nSREBP-1c (as indicated) on the *Acly* and *Acss2* promoter regions (left) or the *Acly* promoter region (right), in livers from control, LiFKO, control + 1c, or LiFKO + 1c mice maintained on normal chow diet (left) or FPC diet (right). Depicted are tracks from 1 representative sample per genotype.

(F) Binding of TFE3 on or near SREBP-1c binding sites ("All peaks"), SREBP-1c binding sites within 5kb of TSSs ("Peaks +/- 5kb TSS"), or SREBP-1c binding sites specifically near TSSs of DNL genes ("Peaks +/- 5kb of DNL gene TSS") in livers from control, LiFKO, control + 1c, or LiFKO + 1c mice maintained on normal chow (n=4; left) or FPC diet (n=3; right). Data are depicted as mean +/- SEM. SREBP-1c binding sites were identified from either publicly available data (GSM2287950; for normal chow) or from the HA-nSREBP-1c ChIP-seq performed in control+1c mice from Fig. 5F (FPC diet).

All binding intensity plots are normalized to 1e7 reads and normalized to each condition's input control.

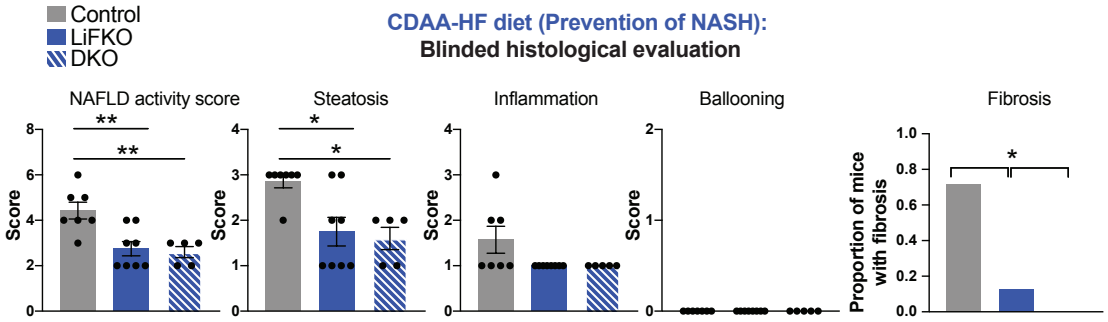
Control
LiFKO
DKO
CDAA-HF diet (Prevention of NASH):
Blinded histological evaluation
NAFLD activity score
Steatosis
Inflammation
Ballooning
Fibrosis
Score
Proportion of mice with fibrosis

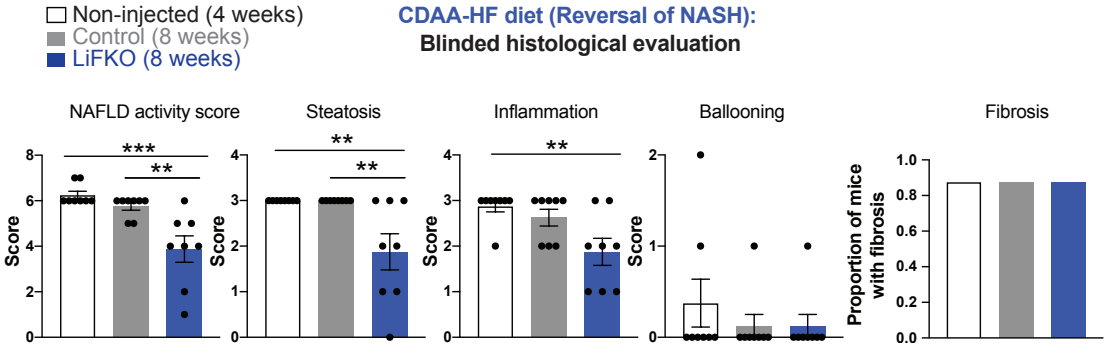
Non-injected (4 weeks)
Control (8 weeks)
LiFKO (8 weeks)
CDAA-HF diet (Reversal of NASH):
Blinded histological evaluation
NAFLD activity score
Steatosis
Inflammation
Ballooning
Fibrosis
Score
Proportion of mice with fibrosis

Fig. S11. Blinded histological evaluation reveals FLCN liver deletion protects mice from NASH

Blinded histological evaluation of liver H&E slides (for NAFLD activity score, steatosis, inflammation, and ballooning) and Sirius Red slides (for fibrosis; livers either exhibited no fibrosis or fibrosis stage 1A), from (A) mice from the prevention of NASH experiment (n=5-8) (Fig. 6A-E) or (B) the reversal of NASH experiment (n=8) (Fig. 6F-J). Fisher's exact test was used to compare number of livers with fibrosis between the genotypes. 1-way ANOVA with Tukey's multiple comparisons test was used for all other statistical analyses. * < p=0.05, ** < p=0.01, *** < p=0.001. Data are depicted as mean +/- SEM.

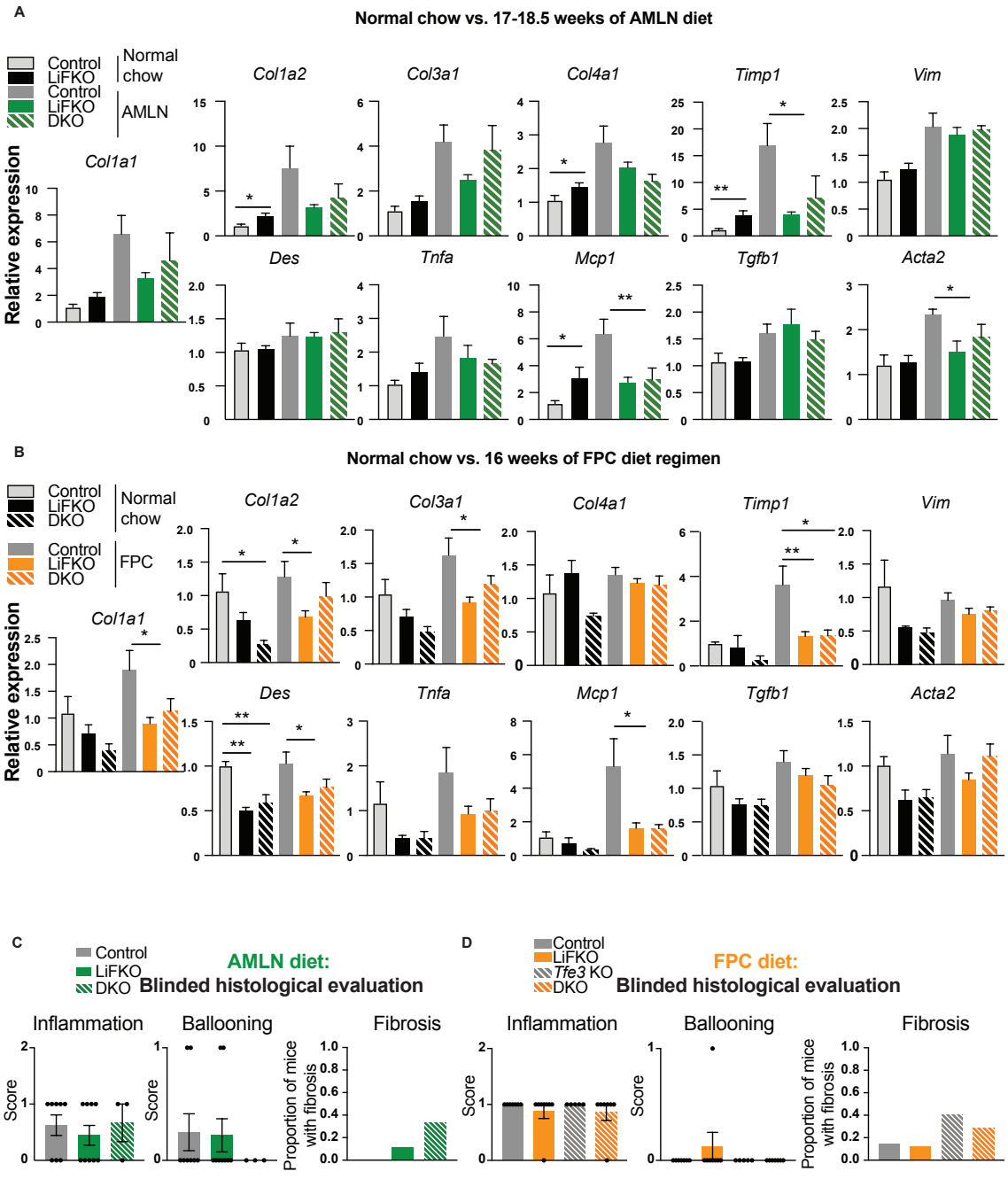
A
Normal chow vs. 17-18.5 weeks of AMLN diet
Control
LiFKO
Normal chow
Control
LiFKO
DKO
AMLN
Relative expression
Col1a1
Col1a2
Col3a1
Col4a1
Timp1
Vim
Des
Tnfa
Mcp1
Tgfb1
Acta2
B
Normal chow vs. 16 weeks of FPC diet regimen
Control
LiFKO
DKO
Normal chow
Control
LiFKO
DKO
FPC
Relative expression
Col1a1
Col1a2
Col3a1
Col4a1
Timp1
Vim
Des
Tnfa
Mcp1
Tgfb1
Acta2
C
Control
LiFKO
DKO
AMLN diet:
Blinded histological evaluation
Inflammation
Ballooning
Fibrosis
Score
Proportion of mice with fibrosis
D
Control
LiFKO
Tfe3 KO
DKO
FPC diet:
Blinded histological evaluation
Inflammation
Ballooning
Fibrosis
Score
Proportion of mice with fibrosis

Fig. S12. FLCN deletion protects mice from NASH in several diets
(A-B) mRNA expression of NASH gene markers in livers of control, LiFKO, and DKO mice fed (A) normal chow (n=7) or 17-18.5 weeks of AMLN diet (n=3-9); or (B) normal chow (n=3) or 16 weeks of FPC diet regimen (TD160785 with sugar water; n=7-11). For normal chow controls for the AMLN diet experiment, student's t-test was used to compare control and LiFKO. In all other conditions, 1-way ANOVA with Tukey's multiple comparisons test was used.
(C-D) Blinded histological evaluation of liver H&E slides (for inflammation and ballooning) and Sirius Red slides (for fibrosis; livers either exhibited no fibrosis or fibrosis stage 1A), from control, LiFKO, *Tfe3* KO, and/or DKO mice fed (C) 17-18.5 weeks of AMLN diet (n=3-9); or (D) 16 weeks of FPC diet regimen (TD160785 with sugar water; n=5-8). For inflammation and ballooning, 1-way ANOVA with Tukey's multiple comparisons test was used. Fisher's exact test was used to compare numbers of livers with fibrosis between the genotypes.
* < p=0.05, ** < p=0.01. Data are depicted as mean +/- SEM.

Table S1. qRT-PCR primers

Gene	Forward	Reverse	Reference (if applicable)
36b4	GGAGCCAGCGAGGCCACACTGCTG	CTGGCCACGTTGCGGACACCCTCC	
Tbp	ACCCTTCACCAATGACTCCTATG	TGACTGCAGCAAATCGCTTGG	
Hprt	GTTAAGCAGTACAGCCCCAAA	AGGGCATATCCAACAACAAACTT	
Srebp1a	GCGCCGGCGCCATGGACGAGCTGGCC	GTTGTTGATGAGCTGGAGCATGTC	
Srebp1c (AMLN diet)	CGGACCACGGAGCCATGGATTGCAC	GTTGTTGATGAGCTGGAGCATGTC	
Srebp1c (all other qRT-PCR experiments)	CGGAGCCATGGATTGCACATT	CTGTCTCACCCCCAGCATAG	
Acly	CAGCCAAGGCAATTTCAGAGC	CTCGACGTTTGATTAACTGGTCT	
Acss2	ACCAGTTAAGAGGCCATGTC	GTACAAGATGAAGAGTGGGTCC	
Fasn	GGAGGTGGTGATAGCCGGTAT	TGGGTAATCCATAGAGCCCAG	
Chrebpa	CGGACTCGGATACGGACTTG	GAAGTGTCCGCTGTGGATGA	
Chrebpb	GAAGGCGCGGGGTGAG	GCTCGGATCCTGGGACCT	
Scd1	GGTGAACAGTGCCGCGCATCTC	GTGTGGTGGTAGTTGTGGAAGCC	
Acaca	ATGGGCGGAATGGTCTCTTTC	TGGGGACCTTGTCTTCATCAT	
Cyp7a1	AGCAACTAAACAACCTGCCAGTACTA	GTCCGGATATTCAAGGATGCA	(*87*)
Abca1	CCCAGAGCAAAAAGCGACTC	GGTCATCATCACTTTGGTCCTTG	(*88*)
Lxra	CAGGCAGGCATGAGGGAG	GAGGAGGTGAGGACACCCTT	
Lxrb	GGTGCAGTCATGAGCCCC	CACGGGAGTGTCCAGAGAAC	
Insig1	TCACAGTGACTGAGCTTCAGCA	TCATCTTCATCACACCCAGGAC	(*89*)
Insig2	CGTGACACTTTTTCCACCAG	GGGTACAACAGCCCAATCAC	(*42*)
Insig2a	CCCTCAATGAATGTACTGAAGGATT	TGTGAAGTGAAGCAGACCAATGT	
Insig2b	CCGGGCAGAGCTCAGGAT	GAAGCAGACCAATGTTTCAATGG	(*89*)
Col1a1	GCTCCTCTTAGGGGCCACT	CCACGTCTCACCATTGGGG	
Col1a2	GTAACTTCGTGCCTAGCAACA	CCTTTGTCAGAATACTGAGCAGC	(*30*)
Col3a1	CCTGGCTCAAATGGCTCAC	CAGGACTGCCGTTATTCCCG	
Col4a1	CTGGCACAAAAGGGACGAG	ACGTGGCCGAGAATTTCACC	(*30*)
Timp1	ATATCCGGTACGCCTACACC	GCCCGTGATGAGAAACTCTT	
Vim	TTTCTCTGCCTCTGCCAAC	TCTCATTGATCACCTGTCCATC	(*30*)
Des	CTAAAGGATGAGATGGCCCG	GAAGGTCTGGATAGGAAGGTTG	(*30*)
Tnfa	CTTCTGTCTACTGAACTTCGGG	CAGGCTTGTCACTCGAATTTTG	(*30*)
Mcp1	TTAAAAACCTGGATCGGAACCAA	GCATTAGCTTCAGATTTACGGGT	(*30*)
Tgfb1	CTCCCGTGGCTTCTAGTGC	GCCTTAGTTTGGACAGGATCTG	(*30*)
Acta2	ATGCTCCCAGGGCTGTTTTCCCAT	GTGGTGCCAGATCTTTTCCATGTCG	(*30*)

References and Notes

1. M. E. Rinella, Nonalcoholic fatty liver disease: A systematic review. *JAMA* **313**, 2263–2273 (2015). doi:10.1001/jama.2015.5370 Medline

2. S. Schuster, D. Cabrera, M. Arrese, A. E. Feldstein, Triggering and resolution of inflammation in NASH. *Nat. Rev. Gastroenterol. Hepatol.* **15**, 349–364 (2018). doi:10.1038/s41575-018-0009-6 Medline

3. R. F. Schwabe, I. Tabas, U. B. Pajvani, Mechanisms of fibrosis development in nonalcoholic steatohepatitis. *Gastroenterology* **158**, 1913–1928 (2020). doi:10.1053/j.gastro.2019.11.311 Medline

4. A. C. Sheka, O. Adeyi, J. Thompson, B. Hameed, P. A. Crawford, S. Ikramuddin, Nonalcoholic steatohepatitis: A review. *JAMA* **323**, 1175–1183 (2020). doi:10.1001/jama.2020.2298 Medline

5. Y. Kawano, D. E. Cohen, Mechanisms of hepatic triglyceride accumulation in non-alcoholic fatty liver disease. *J. Gastroenterol.* **48**, 434–441 (2013). doi:10.1007/s00535-013-0758-5 Medline

6. S. J. H. Ricoult, B. D. Manning, The multifaceted role of mTORC1 in the control of lipid metabolism. *EMBO Rep.* **14**, 242–251 (2013). doi:10.1038/embor.2013.5 Medline

7. C. C. Dibble, B. D. Manning, Signal integration by mTORC1 coordinates nutrient input with biosynthetic output. *Nat. Cell Biol.* **15**, 555–564 (2013). doi:10.1038/ncb2763 Medline

8. T. R. Peterson, S. S. Sengupta, T. E. Harris, A. E. Carmack, S. A. Kang, E. Balderas, D. A. Guertin, K. L. Madden, A. E. Carpenter, B. N. Finck, D. M. Sabatini, mTOR complex 1 regulates lipin 1 localization to control the SREBP pathway. *Cell* **146**, 408–420 (2011). doi:10.1016/j.cell.2011.06.034 Medline

9. T. Porstmann, C. R. Santos, B. Griffiths, M. Cully, M. Wu, S. Leevers, J. R. Griffiths, Y.-L. Chung, A. Schulze, SREBP activity is regulated by mTORC1 and contributes to Akt-dependent cell growth. *Cell Metab.* **8**, 224–236 (2008). doi:10.1016/j.cmet.2008.07.007 Medline

10. H. L. Kenerson, M. M. Yeh, R. S. Yeung, Tuberous sclerosis complex-1 deficiency attenuates diet-induced hepatic lipid accumulation. *PLOS ONE* **6**, e18075 (2011). doi:10.1371/journal.pone.0018075 Medline

11. J. L. Yecies, H. H. Zhang, S. Menon, S. Liu, D. Yecies, A. I. Lipovsky, C. Gorgun, D. J. Kwiatkowski, G. S. Hotamisligil, C.-H. Lee, B. D. Manning, Akt stimulates hepatic SREBP1c and lipogenesis through parallel mTORC1-dependent and independent pathways. *Cell Metab.* **14**, 21–32 (2011). doi:10.1016/j.cmet.2011.06.002 Medline

12. W. J. Quinn 3rd, M. Wan, S. V. Shewale, R. Gelfer, D. J. Rader, M. J. Birnbaum, P. M. Titchenell, mTORC1 stimulates phosphatidylcholine synthesis to promote triglyceride secretion. *J. Clin. Invest.* **127**, 4207–4215 (2017). doi:10.1172/JCI96036 Medline

13. A. Umemura, E. J. Park, K. Taniguchi, J. H. Lee, S. Shalapour, M. A. Valasek, M. Aghajan, H. Nakagawa, E. Seki, M. N. Hall, M. Karin, Liver damage, inflammation, and enhanced

tumorigenesis after persistent mTORC1 inhibition. *Cell Metab.* **20**, 133–144 (2014). doi:10.1016/j.cmet.2014.05.001 Medline

14. S. Wada, M. Neinast, C. Jang, Y. H. Ibrahim, G. Lee, A. Babu, J. Li, A. Hoshino, G. C. Rowe, J. Rhee, J. A. Martina, R. Puertollano, J. Blenis, M. Morley, J. A. Baur, P. Seale, Z. Arany, The tumor suppressor FLCN mediates an alternate mTOR pathway to regulate browning of adipose tissue. *Genes Dev.* **30**, 2551–2564 (2016). doi:10.1101/gad.287953.116 Medline

15. J. Li, S. Wada, L. K. Weaver, C. Biswas, E. M. Behrens, Z. Arany, Myeloid folliculin balances mTOR activation to maintain innate immunity homeostasis. *JCI Insight* **5**, 126939 (2019). doi:10.1172/jci.insight.126939 Medline

16. G. Napolitano, C. Di Malta, A. Esposito, M. E. G. de Araujo, S. Pece, G. Bertalot, M. Matarese, V. Benedetti, A. Zampelli, T. Stasyk, D. Siciliano, A. Venuta, M. Cesana, C. Vilardo, E. Nusco, J. Monfregola, A. Calcagnì, P. P. Di Fiore, L. A. Huber, A. Ballabio, A substrate-specific mTORC1 pathway underlies Birt–Hogg–Dubé syndrome. *Nature* **585**, 597–602 (2020). doi:10.1038/s41586-020-2444-0 Medline

17. L. S. Schmidt, Birt–Hogg–Dubé syndrome: from gene discovery to molecularly targeted therapies. *Fam. Cancer* **12**, 357–364 (2013). doi:10.1007/s10689-012-9574-y Medline

18. Z.-Y. Tsun, L. Bar-Peled, L. Chantranupong, R. Zoncu, T. Wang, C. Kim, E. Spooner, D. M. Sabatini, The folliculin tumor suppressor is a GAP for the RagC/D GTPases that signal amino acid levels to mTORC1. *Mol. Cell* **52**, 495–505 (2013). doi:10.1016/j.molcel.2013.09.016 Medline

19. J. Betschinger, J. Nichols, S. Dietmann, P. D. Corrin, P. J. Paddison, A. Smith, Exit from pluripotency is gated by intracellular redistribution of the bHLH transcription factor Tfe3. *Cell* **153**, 335–347 (2013). doi:10.1016/j.cell.2013.03.012 Medline

20. J. C. Kennedy, D. Khabibullin, T. Hougard, J. Nijmeh, W. Shi, E. P. Henske, Loss of FLCN inhibits canonical WNT signaling via TFE3. *Hum. Mol. Genet.* **28**, 3270–3281 (2019). doi:10.1093/hmg/ddz158 Medline

21. J. C. Kennedy, D. Khabibullin, Y. Boku, W. Shi, E. P. Henske, New developments in the pathogenesis of pulmonary cysts in Birt–Hogg–Dubé Syndrome. *Semin. Respir. Crit. Care Med.* **41**, 247–255 (2020). doi:10.1055/s-0040-1708500 Medline

22. S.-B. Hong, H. Oh, V. A. Valera, M. Baba, L. S. Schmidt, W. M. Linehan, Inactivation of the *FLCN* tumor suppressor gene induces TFE3 transcriptional activity by increasing its nuclear localization. *PLOS ONE* **5**, e15793 (2010). doi:10.1371/journal.pone.0015793 Medline

23. M. Yan, É. Audet-Walsh, S. Manteghi, C. R. Dufour, B. Walker, M. Baba, J. St-Pierre, V. Giguère, A. Pause, Chronic AMPK activation via loss of FLCN induces functional beige adipose tissue through PGC-1α/ERRα. *Genes Dev.* **30**, 1034–1046 (2016). doi:10.1101/gad.281410.116 Medline

24. M. Baba, S.-B. Hong, N. Sharma, M. B. Warren, M. L. Nickerson, A. Iwamatsu, D. Esposito, W. K. Gillette, R. F. Hopkins 3rd, J. L. Hartley, M. Furihata, S. Oishi, W. Zhen, T. R. Burke Jr., W. M. Linehan, L. S. Schmidt, B. Zbar, Folliculin encoded by the *BHD* gene interacts with a binding protein, FNIP1, and AMPK, and is involved in AMPK and

mTOR signaling. *Proc. Natl. Acad. Sci. U.S.A.* **103**, 15552–15557 (2006). doi:10.1073/pnas.0603781103 Medline

25. D. Khabibullin, D. A. Medvetz, M. Pinilla, V. Hariharan, C. Li, A. Hergrueter, M. Laucho Contreras, E. Zhang, A. Parkhitko, J. J. Yu, C. A. Owen, H. Huang, R. M. Baron, E. P. Henske, Folliculin regulates cell–cell adhesion, AMPK, and mTORC1 in a cell-type-specific manner in lung-derived cells. *Physiol. Rep.* **2**, e12107 (2014). doi:10.14814/phy2.12107 Medline

26. M. Yan, M.-C. Gingras, E. A. Dunlop, Y. Nouët, F. Dupuy, Z. Jalali, E. Possik, B. J. Coull, D. Kharitidi, A. B. Dydensborg, B. Faubert, M. Kamps, S. Sabourin, R. S. Preston, D. M. Davies, T. Roughead, L. Chotard, M. A. M. van Steensel, R. Jones, A. R. Tee, A. Pause, The tumor suppressor folliculin regulates AMPK-dependent metabolic transformation. *J. Clin. Invest.* **124**, 2640–2650 (2014). doi:10.1172/JCI71749 Medline

27. A. R. Tee, B. D. Manning, P. P. Roux, L. C. Cantley, J. Blenis, Tuberous sclerosis complex gene products, Tuberin and Hamartin, control mTOR signaling by acting as a GTPase-activating protein complex toward Rheb. *Curr. Biol.* **13**, 1259–1268 (2003). doi:10.1016/S0960-9822(03)00506-2 Medline

28. J. R. Clapper, M. D. Hendricks, G. Gu, C. Wittmer, C. S. Dolman, J. Herich, J. Athanacio, C. Villescaz, S. S. Ghosh, J. S. Heilig, C. Lowe, J. D. Roth, Diet-induced mouse model of fatty liver disease and nonalcoholic steatohepatitis reflecting clinical disease progression and methods of assessment. *Am. J. Physiol. Gastrointest. Liver Physiol.* **305**, G483–G495 (2013). doi:10.1152/ajpgi.00079.2013 Medline

29. M. L. Boland, D. Oró, K. S. Tølbøl, S. T. Thrane, J. C. Nielsen, T. S. Cohen, D. E. Tabor, F. Fernandes, A. Tovchigrechko, S. S. Veidal, P. Warrener, B. R. Sellman, J. Jelsing, M. Feigh, N. Vrang, J. L. Trevaskis, H. H. Hansen, Towards a standard diet-induced and biopsy-confirmed mouse model of non-alcoholic steatohepatitis: Impact of dietary fat source. *World J. Gastroenterol.* **25**, 4904–4920 (2019). doi:10.3748/wjg.v25.i33.4904 Medline

30. X. Wang, Z. Zheng, J. M. Caviglia, K. E. Corey, T. M. Herfel, B. Cai, R. Masia, R. T. Chung, J. H. Lefkowitch, R. F. Schwabe, I. Tabas, Hepatocyte TAZ/WWTR1 promotes inflammation and fibrosis in nonalcoholic steatohepatitis. *Cell Metab.* **24**, 848–862 (2016). doi:10.1016/j.cmet.2016.09.016 Medline

31. R. L. Jacobs, Y. Zhao, D. P. Y. Koonen, T. Sletten, B. Su, S. Lingrell, G. Cao, D. A. Peake, M.-S. Kuo, S. D. Proctor, B. P. Kennedy, J. R. B. Dyck, D. E. Vance, Impaired *de novo* choline synthesis explains why phosphatidylethanolamine *N*-methyltransferase-deficient mice are protected from diet-induced obesity. *J. Biol. Chem.* **285**, 22403–22413 (2010). doi:10.1074/jbc.M110.108514 Medline

32. J. A. Martina, H. I. Diab, L. Lishu, L. Jeong-A, S. Patange, N. Raben, R. Puertollano, The nutrient-responsive transcription factor TFE3 promotes autophagy, lysosomal biogenesis, and clearance of cellular debris. *Sci. Signal.* **7**, ra9 (2014). doi:10.1126/scisignal.2004754 Medline

33. J. Xiong, K. Wang, J. He, G. Zhang, D. Zhang, F. Chen, *TFE3* alleviates hepatic steatosis through autophagy-induced lipophagy and *PGC1α*-mediated fatty acid β-oxidation. *Int. J. Mol. Sci.* **17**, 387 (2016). doi:10.3390/ijms17030387 Medline

34. J. C. Yoon, P. Puigserver, G. Chen, J. Donovan, Z. Wu, J. Rhee, G. Adelmant, J. Stafford, C. R. Kahn, D. K. Granner, C. B. Newgard, B. M. Spiegelman, Control of hepatic gluconeogenesis through the transcriptional coactivator PGC-1. *Nature* **413**, 131–138 (2001). doi:10.1038/35093050 Medline

35. Y. Wang, J. Viscarra, S.-J. Kim, H. S. Sul, Transcriptional regulation of hepatic lipogenesis. *Nat. Rev. Mol. Cell Biol.* **16**, 678–689 (2015). doi:10.1038/nrm4074 Medline

36. M. Gao, D. Liu, The liver X receptor agonist T0901317 protects mice from high fat diet-induced obesity and insulin resistance. *AAPS J.* **15**, 258–266 (2013). doi:10.1208/s12248-012-9429-3 Medline

37. J. D. Horton, J. L. Goldstein, M. S. Brown, SREBPs: Activators of the complete program of cholesterol and fatty acid synthesis in the liver. *J. Clin. Invest.* **109**, 1125–1131 (2002). doi:10.1172/JCI0215593 Medline

38. D. Yabe, M. S. Brown, J. L. Goldstein, Insig-2, a second endoplasmic reticulum protein that binds SCAP and blocks export of sterol regulatory element-binding proteins. *Proc. Natl. Acad. Sci. U.S.A.* **99**, 12753–12758 (2002). doi:10.1073/pnas.162488899 Medline

39. G. Le Martelot, T. Claudel, D. Gatfield, O. Schaad, B. Kornmann, G. Lo Sasso, A. Moschetta, U. Schibler, REV-ERBα participates in circadian SREBP signaling and bile acid homeostasis. *PLOS Biol.* **7**, e1000181 (2009). doi:10.1371/journal.pbio.1000181 Medline

40. D. Guan, Y. Xiong, P. C. Borck, C. Jang, P.-T. Doulias, R. Papazyan, B. Fang, C. Jiang, Y. Zhang, E. R. Briggs, W. Hu, D. Steger, H. Ischiropoulos, J. D. Rabinowitz, M. A. Lazar, Diet-induced circadian enhancer remodeling synchronizes opposing hepatic lipid metabolic processes. *Cell* **174**, 831–842.e12 (2018). doi:10.1016/j.cell.2018.06.031 Medline

41. C. R. Yellaturu, X. Deng, E. A. Park, R. Raghow, M. B. Elam, Insulin enhances the biogenesis of nuclear sterol regulatory element-binding protein (SREBP)-1c by posttranscriptional down-regulation of Insig-2A and its dissociation from SREBP cleavage-activating protein (SCAP)·SREBP-1c complex. *J. Biol. Chem.* **284**, 31726–31734 (2009). doi:10.1074/jbc.M109.050914 Medline

42. R. Papazyan, Z. Sun, Y. H. Kim, P. M. Titchenell, D. A. Hill, W. Lu, M. Damle, M. Wan, Y. Zhang, E. R. Briggs, J. D. Rabinowitz, M. A. Lazar, Physiological suppression of lipotoxic liver damage by complementary actions of HDAC3 and SCAP/SREBP. *Cell Metab.* **24**, 863–874 (2016). doi:10.1016/j.cmet.2016.10.012 Medline

43. C. Settembre, C. Di Malta, V. A. Polito, M. Garcia Arencibia, F. Vetrini, S. Erdin, S. U. Erdin, T. Huynh, D. Medina, P. Colella, M. Sardiello, D. C. Rubinsztein, A. Ballabio, TFEB links autophagy to lysosomal biogenesis. *Science* **332**, 1429–1433 (2011). doi:10.1126/science.1204592 Medline

44. J. D. Horton, Y. Bashmakov, I. Shimomura, H. Shimano, Regulation of sterol regulatory element binding proteins in livers of fasted and refed mice. *Proc. Natl. Acad. Sci. U.S.A.* **95**, 5987–5992 (1998). doi:10.1073/pnas.95.11.5987 Medline

45. E. Steingrímsson, L. Tessarollo, B. Pathak, L. Hou, H. Arnheiter, N. G. Copeland, N. A. Jenkins, Mitf and Tfe3, two members of the Mitf-Tfe family of bHLH-Zip transcription

factors, have important but functionally redundant roles in osteoclast development. *Proc. Natl. Acad. Sci. U.S.A.* **99**, 4477–4482 (2002). doi:10.1073/pnas.072071099 Medline

46. P. Angulo, D. E. Kleiner, S. Dam-Larsen, L. A. Adams, E. S. Bjornsson, P. Charatcharoenwitthaya, P. R. Mills, J. C. Keach, H. D. Lafferty, A. Stahler, S. Haflidadottir, F. Bendtsen, Liver fibrosis, but no other histologic features, is associated with long-term outcomes of patients with nonalcoholic fatty liver disease. *Gastroenterology* **149**, 389–397.e10 (2015). doi:10.1053/j.gastro.2015.04.043 Medline

47. M. Matsumoto, N. Hada, Y. Sakamaki, A. Uno, T. Shiga, C. Tanaka, T. Ito, A. Katsume, M. Sudoh, An improved mouse model that rapidly develops fibrosis in non-alcoholic steatohepatitis. *Int. J. Exp. Pathol.* **94**, 93–103 (2013). doi:10.1111/iep.12008 Medline

48. G. Wei, P. An, K. A. Vaid, I. Nasser, P. Huang, L. Tan, S. Zhao, D. Schuppan, Y. V. Popov, Comparison of murine steatohepatitis models identifies a dietary intervention with robust fibrosis, ductular reaction, and rapid progression to cirrhosis and cancer. *Am. J. Physiol. Gastrointest. Liver Physiol.* **318**, G174–G188 (2020). doi:10.1152/ajpgi.00041.2019 Medline

49. K. A. Lytle, D. B. Jump, Is Western diet-induced nonalcoholic steatohepatitis in *Ldlr*$^{-/-}$ mice reversible? *PLOS ONE* **11**, e0146942 (2016). doi:10.1371/journal.pone.0146942 Medline

50. C. D. Vocke, Y. Yang, C. P. Pavlovich, L. S. Schmidt, M. L. Nickerson, C. A. Torres-Cabala, M. J. Merino, M. M. Walther, B. Zbar, W. M. Linehan, High frequency of somatic frameshift BHD gene mutations in Birt–Hogg–Dubé-associated renal tumors. *J. Natl. Cancer Inst.* **97**, 931–935 (2005). doi:10.1093/jnci/dji154 Medline

51. A. A. Barba, S. Bochicchio, A. Dalmoro, G. Lamberti, Lipid delivery systems for nucleic-acid-based-drugs: From production to clinical applications. *Pharmaceutics* **11**, 360 (2019). doi:10.3390/pharmaceutics11080360 Medline

52. A. J. Debacker, J. Voutila, M. Catley, D. Blakey, N. Habib, Delivery of oligonucleotides to the liver with GalNAc: From research to registered therapeutic drug. *Mol. Ther.* **28**, 1759–1771 (2020). doi:10.1016/j.ymthe.2020.06.015 Medline

53. J. Rüger, S. Ioannou, D. Castanotto, C. A. Stein, Oligonucleotides to the (gene) rescue: FDA approvals 2017–2019. *Trends Pharmacol. Sci.* **41**, 27–41 (2020). doi:10.1016/j.tips.2019.10.009 Medline

54. M. Baba, M. Furihata, S.-B. Hong, L. Tessarollo, D. C. Haines, E. Southon, V. Patel, P. Igarashi, W. G. Alvord, R. Leighty, M. Yao, M. Bernardo, L. Ileva, P. Choyke, M. B. Warren, B. Zbar, W. M. Linehan, L. S. Schmidt, Kidney-targeted Birt-Hogg-Dubé gene inactivation in a mouse model: Erk1/2 and Akt-mTOR activation, cell hyperproliferation, and polycystic kidneys. *J. Natl. Cancer Inst.* **100**, 140–154 (2008). doi:10.1093/jnci/djm288 Medline

55. V. Hudon, S. Sabourin, A. B. Dydensborg, V. Kottis, A. Ghazi, M. Paquet, K. Crosby, V. Pomerleau, N. Uetani, A. Pause, Renal tumour suppressor function of the Birt–Hogg–Dubé syndrome gene product folliculin. *J. Med. Genet.* **47**, 182–189 (2010). doi:10.1136/jmg.2009.072009 Medline

56. A. Hagiwara, M. Cornu, N. Cybulski, P. Polak, C. Betz, F. Trapani, L. Terracciano, M. H. Heim, M. A. Rüegg, M. N. Hall, Hepatic mTORC2 activates glycolysis and lipogenesis

through Akt, glucokinase, and SREBP1c. *Cell Metab.* **15**, 725–738 (2012). doi:10.1016/j.cmet.2012.03.015 Medline

57. M. Yuan, E. Pino, L. Wu, M. Kacergis, A. A. Soukas, Identification of Akt-independent regulation of hepatic lipogenesis by mammalian target of rapamycin (mTOR) complex 2. *J. Biol. Chem.* **287**, 29579–29588 (2012). doi:10.1074/jbc.M112.386854 Medline

58. N. Bhat, A. Narayanan, M. Fathzadeh, M. Kahn, D. Zhang, L. Goedeke, A. Neogi, R. L. Cardone, R. G. Kibbey, C. Fernandez-Hernando, H. N. Ginsberg, D. Jain, G. I. Shulman, A. Mani, Dyrk1b promotes hepatic lipogenesis by bypassing canonical insulin signaling and directly activating mTORC2 in mice. *J. Clin. Invest.* **132**, 153724 (2022). Medline

59. K. L. Donnelly, C. I. Smith, S. J. Schwarzenberg, J. Jessurun, M. D. Boldt, E. J. Parks, Sources of fatty acids stored in liver and secreted via lipoproteins in patients with nonalcoholic fatty liver disease. *J. Clin. Invest.* **115**, 1343–1351 (2005). doi:10.1172/JCI23621 Medline

60. J. E. Lambert, M. A. Ramos-Roman, J. D. Browning, E. J. Parks, Increased de novo lipogenesis is a distinct characteristic of individuals with nonalcoholic fatty liver disease. *Gastroenterology* **146**, 726–735 (2014). doi:10.1053/j.gastro.2013.11.049 Medline

61. C.-W. Kim, C. Addy, J. Kusunoki, N. N. Anderson, S. Deja, X. Fu, S. C. Burgess, C. Li, M. Ruddy, M. Chakravarthy, S. Previs, S. Milstein, K. Fitzgerald, D. E. Kelley, J. D. Horton, Acetyl CoA carboxylase inhibition reduces hepatic steatosis but elevates plasma triglycerides in mice and humans: A bedside to bench investigation. *Cell Metab.* **26**, 394–406.e6 (2017). doi:10.1016/j.cmet.2017.07.009 Medline

62. S. L. Friedman, B. A. Neuschwander-Tetri, M. Rinella, A. J. Sanyal, Mechanisms of NAFLD development and therapeutic strategies. *Nat. Med.* **24**, 908–922 (2018). doi:10.1038/s41591-018-0104-9 Medline

63. Y. Hu, I. Semova, X. Sun, H. Kang, S. Chahar, A. N. Hollenberg, D. Masson, M. D. Hirschey, J. Miao, S. B. Biddinger, Fructose and glucose can regulate mammalian target of rapamycin complex 1 and lipogenic gene expression via distinct pathways. *J. Biol. Chem.* **293**, 2006–2014 (2018). doi:10.1074/jbc.M117.782557 Medline

64. B. D. Hegarty, A. Bobard, I. Hainault, P. Ferré, P. Bossard, F. Foufelle, Distinct roles of insulin and liver X receptor in the induction and cleavage of sterol regulatory element-binding protein-1c. *Proc. Natl. Acad. Sci. U.S.A.* **102**, 791–796 (2005). doi:10.1073/pnas.0405067102 Medline

65. D. E. Kleiner, E. M. Brunt, M. Van Natta, C. Behling, M. J. Contos, O. W. Cummings, L. D. Ferrell, Y.-C. Liu, M. S. Torbenson, A. Unalp-Arida, M. Yeh, A. J. McCullough, A. J. Sanyal; Nonalcoholic Steatohepatitis Clinical Research Network, Design and validation of a histological scoring system for nonalcoholic fatty liver disease. *Hepatology* **41**, 1313–1321 (2005). doi:10.1002/hep.20701 Medline

66. A. I. Mina, R. A. LeClair, K. B. LeClair, D. E. Cohen, L. Lantier, A. S. Banks, *CalR*: A web-based analysis tool for indirect calorimetry experiments. *Cell Metab.* **28**, 656–666.e1 (2018). doi:10.1016/j.cmet.2018.06.019 Medline

67. A. M. Bolger, M. Lohse, B. Usadel, Trimmomatic: A flexible trimmer for Illumina sequence data. *Bioinformatics* **30**, 2114–2120 (2014). doi:10.1093/bioinformatics/btu170 Medline

68. A. Dobin, C. A. Davis, F. Schlesinger, J. Drenkow, C. Zaleski, S. Jha, P. Batut, M. Chaisson, T. R. Gingeras, STAR: Ultrafast universal RNA-seq aligner. *Bioinformatics* **29**, 15–21 (2013). doi:10.1093/bioinformatics/bts635 Medline

69. H. Li, B. Handsaker, A. Wysoker, T. Fennell, J. Ruan, N. Homer, G. Marth, G. Abecasis, R. Durbin; 1000 Genome Project Data Processing Subgroup, The Sequence Alignment/Map format and SAMtools. *Bioinformatics* **25**, 2078–2079 (2009). doi:10.1093/bioinformatics/btp352 Medline

70. Y. Liao, G. K. Smyth, W. Shi, The R package *Rsubread* is easier, faster, cheaper and better for alignment and quantification of RNA sequencing reads. *Nucleic Acids Res.* **47**, e47 (2019). doi:10.1093/nar/gkz114 Medline

71. M. E. Ritchie, B. Phipson, D. Wu, Y. Hu, C. W. Law, W. Shi, G. K. Smyth, *limma* powers differential expression analyses for RNA-sequencing and microarray studies. *Nucleic Acids Res.* **43**, e47 (2015). doi:10.1093/nar/gkv007 Medline

72. D. Wu, G. K. Smyth, Camera: A competitive gene set test accounting for inter-gene correlation. *Nucleic Acids Res.* **40**, e133 (2012). doi:10.1093/nar/gks461 Medline

73. K. Blighe, L. DeDionisio, K. A. Christie, B. Chawes, S. Shareef, T. Kakouli-Duarte, C. Chao-Shern, V. Harding, R. S. Kelly, L. Castellano, J. Stebbing, J. A. Lasky-Su, M. A. Nesbit, C. B. T. Moore, Gene editing in the context of an increasingly complex genome. *BMC Genomics* **19**, 595 (2018). doi:10.1186/s12864-018-4963-8 Medline

74. M. Moskot, J. Jakóbkiewicz-Banecka, A. Kloska, E. Smolińska, P. Mozolewski, M. Malinowska, M. Rychłowski, B. Banecki, G. Węgrzyn, M. Gabig-Cimińska, Modulation of expression of genes involved in glycosaminoglycan metabolism and lysosome biogenesis by flavonoids. *Sci. Rep.* **5**, 9378 (2015). doi:10.1038/srep09378 Medline

75. A. Fabregat, K. Sidiropoulos, G. Viteri, O. Forner, P. Marin-Garcia, V. Arnau, P. D'Eustachio, L. Stein, H. Hermjakob, Reactome pathway analysis: A high-performance in-memory approach. *BMC Bioinformatics* **18**, 142 (2017). doi:10.1186/s12859-017-1559-2 Medline

76. C. Jang, S. Wada, S. Yang, B. Gosis, X. Zeng, Z. Zhang, Y. Shen, G. Lee, Z. Arany, J. D. Rabinowitz, The small intestine shields the liver from fructose-induced steatosis. *Nat. Metab.* **2**, 586–593 (2020). doi:10.1038/s42255-020-0222-9 Medline

77. T. Plösch, "The ABC of cholesterol transport," thesis, University of Groningen (2004).

78. M. Abu-Remaileh, G. A. Wyant, C. Kim, N. N. Laqtom, M. Abbasi, S. H. Chan, E. Freinkman, D. M. Sabatini, Lysosomal metabolomics reveals V-ATPase- and mTOR-dependent regulation of amino acid efflux from lysosomes. *Science* **358**, 807–813 (2017). doi:10.1126/science.aan6298 Medline

79. M. Mano, R. Ippodrino, L. Zentilin, S. Zacchigna, M. Giacca, Genome-wide RNAi screening identifies host restriction factors critical for in vivo AAV transduction. *Proc. Natl. Acad. Sci. U.S.A.* **112**, 11276–11281 (2015). doi:10.1073/pnas.1503607112 Medline

80. B. Langmead, S. L. Salzberg, Fast gapped-read alignment with Bowtie 2. *Nat. Methods* **9**, 357–359 (2012). doi:10.1038/nmeth.1923 Medline

81. A. R. Quinlan, I. M. Hall, BEDTools: A flexible suite of utilities for comparing genomic features. *Bioinformatics* **26**, 841–842 (2010). doi:10.1093/bioinformatics/btq033 Medline

82. H. M. Amemiya, A. Kundaje, A. P. Boyle, The ENCODE Blacklist: Identification of problematic regions of the genome. *Sci. Rep.* **9**, 9354 (2019). doi:10.1038/s41598-019-45839-z Medline

83. S. Heinz, C. Benner, N. Spann, E. Bertolino, Y. C. Lin, P. Laslo, J. X. Cheng, C. Murre, H. Singh, C. K. Glass, Simple combinations of lineage-determining transcription factors prime *cis*-regulatory elements required for macrophage and B cell identities. *Mol. Cell* **38**, 576–589 (2010). doi:10.1016/j.molcel.2010.05.004 Medline

84. W. J. Kent, A. S. Zweig, G. Barber, A. S. Hinrichs, D. Karolchik, BigWig and BigBed: enabling browsing of large distributed datasets. *Bioinformatics* **26**, 2204–2207 (2010). doi:10.1093/bioinformatics/btq351 Medline

85. X. Zhou, B. Maricque, M. Xie, D. Li, V. Sundaram, E. A. Martin, B. C. Koebbe, C. Nielsen, M. Hirst, P. Farnham, R. M. Kuhn, J. Zhu, I. Smirnov, W. J. Kent, D. Haussler, P. A. F. Madden, J. F. Costello, T. Wang, The Human Epigenome Browser at Washington University. *Nat. Methods* **8**, 989–990 (2011). doi:10.1038/nmeth.1772 Medline

86. F. Ramírez, D. P. Ryan, B. Grüning, V. Bhardwaj, F. Kilpert, A. S. Richter, S. Heyne, F. Dündar, T. Manke, deepTools2: A next generation web server for deep-sequencing data analysis. *Nucleic Acids Res.* **44**, W160–W165 (2016). doi:10.1093/nar/gkw257 Medline

87. V. C. Reese, D. D. Moore, A. McLachlan, Limited effects of bile acids and small heterodimer partner on hepatitis B virus biosynthesis *in vivo*. *J. Virol.* **86**, 2760–2768 (2012). doi:10.1128/JVI.06742-11 Medline

88. Z. Huang, N. Liang, A. Damdimopoulos, R. Fan, E. Treuter, G protein pathway suppressor 2 (GPS2) links inflammation and cholesterol efflux by controlling lipopolysaccharide-induced ATP-binding cassette transporter A1 expression in macrophages. *FASEB J.* **33**, 1631–1643 (2019). doi:10.1096/fj.201801123R Medline

89. D. Yabe, R. Komuro, G. Liang, J. L. Goldstein, M. S. Brown, Liver-specific mRNA for Insig-2 down-regulated by insulin: Implications for fatty acid synthesis. *Proc. Natl. Acad. Sci. U.S.A.* **100**, 3155–3160 (2003). doi:10.1073/pnas.0130116100 Medline